Blood Flow

C. Alberto Figueroa[1], Charles A. Taylor[2] and Alison L. Marsden[3]

[1]*Departments of Biomedical Engineering and Surgery, University of Michigan, Ann Arbor, MI, USA*
[2]*HeartFlow Inc., Redwood City, CA, USA*
[3]*Departments of Pediatrics and Bioengineering, Stanford University, Stanford, CA, USA*

1 INTRODUCTION

The cardiovascular system transports gases (oxygen and carbon dioxide), nutrients, enzymes, hormones, and heat between the respiratory, digestive, endocrine, and excretory systems and the cells of the body. It is the inherent scale-linking mechanism between organ system and cellular scales. Far from a static system, the cardiovascular system continually changes and adapts to meet the demands of the organism in healthy and diseased states. Hemodynamic (blood fluid mechanic) factors including flow rate, shear stress, and pressure forces provide the stimuli for many acute and chronic biologic adaptations.

Local hemodynamic factors often act as stimuli to trigger changes in cardiac output and downstream vascular resistance that are essential in responding to acute changes in organ demand. For example, during exercise, the blood flow rate established to meet the metabolic demands of resting conditions is insufficient for the active muscles. These muscles release metabolic products that cause the local vessels to dilate, resulting in a decrease in the local vascular resistance and an increase in muscle blood flow by shunting blood from other tissues and organs. The blood vessels upstream of those in the working muscle in turn dilate because of increased flow. This mechanism is hypothesized to be modulated by increased shear stress triggering the release of nitric oxide from the endothelial cells lining the inner surface of blood vessels experiencing increased flow. Ultimately, the dilation of the vascular bed supplying the working muscles reduces the overall vascular resistance felt by the heart and would reduce systemic blood pressure if the cardiac output remained constant. Instead, baroreceptors, specialized pressure-sensing cells in the aorta and carotid arteries, provide feedback to the nervous system to increase heart rate and cardiac output to maintain blood pressure. While blood flow rate can increase several-fold during exercise conditions, mean blood pressure typically changes by less than 10–20%. In summary, the hemodynamic variables of flow rate, shear stress, and blood pressure all play a role in the response of the cardiovascular system to acute changes in end-organ demand. Quantifying these variables under a range of physiologic conditions is one of the important applications of computational methods applied to model blood flow.

The cardiovascular system also adapts to long-term anatomic and physiologic changes of the organism as occurs during growth, aging, injury, increased or decreased physical activity levels, and the onset of disease. Again, hemodynamic conditions play important roles in vascular adaptation

Encyclopedia of Computational Mechanics Second Edition,
Edited by Erwin Stein, René de Borst and Thomas J.R. Hughes.

DOI: 10.1002/9781119176817.ecm2068

in health and disease. Changes in blood velocity and pressure fields, sensed at a cellular level, initiate a cascade of biochemical signals leading to hierarchical reorganization across molecular, cellular, tissue, and system scales (Humphrey, 2008). For example, blood vessels enlarge in response to chronic increases in blood flow through a mechanism thought to be modulated by increased shear stress acting on the endothelial cells (Kamiya and Togawa, 1980; Zarins *et al.*, 1987). In contrast to vascular enlargement in response to increased flow, blood vessels reduce in caliber in response to reductions in blood flow (Galt *et al.*, 1993). In addition to shear-modulated changes in the diameter of blood vessels due to changes in blood flow, the walls of blood vessels get thinner as a result of decreased pressure and thicken in response to increased pressure through a mechanism hypothesized to be modulated by changes in tensile stress (Liu and Fung, 1989). These adaptive processes are part of a growing body of research on vascular growth and remodeling (G&R), which will be described in the following sections (Figueroa *et al.*, 2009; Sankaran *et al.*, 2013; Valentín and Humphrey, 2009).

Computational methods have been widely applied to the quantification of hemodynamic and biomechanical factors in relation to the genesis, progression, and clinical consequences of congenital and acquired cardiovascular disease. Congenital cardiovascular diseases arise from structural abnormalities of the heart and blood vessels including septal defects (holes between the atria or ventricles), obstructions of the valves of the heart or major arteries leaving the heart, transposition of the major arteries exiting the heart, and inadequate development of the right or left ventricles. In some cases, multiple defects are present or one defect can precipitate another, as occurs when obstruction of the tricuspid valve (between the right atrium and ventricle) interferes with the normal development of the right ventricle. As in the case of the normal adaptation of blood vessels in response to changes in shear or tensile stress, hemodynamic factors play an important role in the development and progression of congenital cardiovascular disease. Further, since reconstructive surgeries or catheter-based interventions used to repair congenital malformations alter the hemodynamic conditions, methods to model blood flow, coupled to cardiovascular physiology, have increasing application in clinical decision-making in pediatric cardiology and surgery (Yang *et al.*, 2011; Baretta *et al.*, 2011; Hsia *et al.*, 2011; Ensley *et al.*, 2000b).

Acquired cardiovascular disease became the leading cause of death in the industrialized world in the early twentieth century and contributes to roughly a third of global deaths. The most predominant form of acquired cardiovascular disease, atherosclerosis, results from the chronic buildup of fatty material in the inner layer of the arteries supplying the heart, brain, kidneys, digestive system, and lower extremities. Interestingly, the upper extremity vessels are typically spared of atherosclerosis. Risk factors for atherosclerosis including smoking, high cholesterol diet, physical inactivity, and obesity affect all the arteries of the body, but notably, the disease is localized at branches and bends of the arterial tree. The observation that atherosclerosis occurs only in localized regions of the body has led to the hypothesis that hemodynamic factors play a critical role in its development (Zarins *et al.*, 1983; Caro *et al.*, 1971; Friedman *et al.*, 1981). This has motivated the application of experimental and computational methods to quantify hemodynamics and vessel wall biomechanics in human arteries. This will be discussed further in the remainder of this chapter.

In contrast to occlusive diseases such as atherosclerosis that results in vessel narrowing, aneurysmal disease results in vessel enlargement and in some cases rupture. As in the case of atherosclerosis, despite risk factors that are diffuse throughout the body, aneurysmal disease is highly localized and occurs predominantly in the aorta, and the iliac, popliteal, carotid, and cerebral arteries, and can occur in the coronary arteries as a result of Kawasaki disease. The localization of aneurysmal disease is hypothesized to be influenced by hemodynamic conditions including flow stagnation and pressure wave amplification. For example, one of the most common sites of aneurysmal disease, the infrarenal abdominal aorta, is a location where blood flow is particularly complex and recirculating as a result of the multiple branches that deliver blood to the organs in the abdomen (Ku, 1994; Xu *et al.*, 1994; Taylor *et al.*, 1998a, 1999, 2002). The resulting flow stagnation in the infrarenal abdominal aorta may enhance inflammatory processes hypothesized to contribute to the degradation of the vessel wall. In addition, because of the reduction of cross-sectional area and progressive stiffening of the aorta from the heart to the pelvis, as well as pressure reflections from downstream vessels, the pressure pulse increases in magnitude and contributes to a greater load on the wall of the abdominal aorta. Once again, the quantification of blood flow velocity and pressure fields may contribute to investigations into the pathogenesis of aneurysmal disease.

Finally, in clinical medicine, the quantification of blood flow velocity and pressure fields is becoming increasingly important in the diagnosis, treatment planning, and subsequent management of patients with congenital and acquired cardiovascular diseases. Risk stratification may be enabled using computational modeling to augment clinical imaging studies, providing hemodynamic data that may be otherwise unattainable. One such technology, $\mathrm{FF}R_{CT}$, which is already gaining traction in the clinic for the evaluation of functional significance of coronary lesions, was recently approved for clinical use by the US Food and Drug Administration

(FDA). Medical, interventional, and surgical therapies used to increase or restore blood flow to compromised organs and tissues or isolate aneurysmal regions from pressure forces may benefit from quantitative data provided by computational methods.

This chapter is focused on computational methods for quantifying blood flow velocity and pressure fields in human arteries and is organized as follows. Section 2 provides a concise overview of important concepts from cardiovascular anatomy and physiology. Section 3 summarizes several well-established methods in blood flow modeling, including the paradigm of image-based modeling, zero-dimensional (0D) (i.e., lumped parameter) models, one-dimensional (1D) theory, three-dimensional methods, and fluid–structure interaction (FSI) formulations. Section 4 explores novel computational tools for blood flow modeling, including formulations for tissue G&R, methods for parameter estimation and uncertainty quantification (UQ), and optimization. Section 5 focuses on several important clinical applications, namely, pediatric cardiology, coronary artery disease, and simulation of transitional hemodynamic stages. Finally, Section 6 describes some of the important areas of future development and challenges anticipated for computational modeling of cardiovascular blood flow.

2 OVERVIEW OF THE CARDIOVASCULAR SYSTEM

The circulatory system is the primary means of transport for oxygen, nutrients, and hormones in organisms. The key elements of all closed circulatory systems are a circulating fluid (blood), a pumping mechanism (heart), a distribution system (arteries), an exchange system (capillaries), and a collection system (veins). Note that some animals, notably insects, and many mollusks, eject a blood-like fluid directly into their body cavities. This open circulatory system, operating under low pressures and small velocities, is a relatively inefficient transport system that poses great difficulties for the organism in achieving a differential distribution of blood flow to various organs and tissues (Kay, 1998). Here, we focus our attention on mammalian circulatory systems. The interested reader is referred to the following books (Kay, 1998; Kardong, 2002) for further discussion of circulatory systems in other animals.

Blood is a suspension of cells in plasma. The concentration of cells, termed the hematocrit, is approximately 50% by volume but may vary in diseased states. We can distinguish three major types of cells on the basis of their function in the circulation: erythrocytes, leukocytes, and thrombocytes. Erythrocytes or red blood cells are the most abundant cells in the blood stream (and the body) and are the primary transport vessels for oxygen and carbon dioxide. It is estimated that of the approximately 100 trillion cells in the body, fully one-fourth are erythrocytes. Mammalian erythrocytes are disk shaped (due to the absence of a nucleus) with a diameter of approximately 8μm and a thickness of 2μm. Leukocytes or white blood cells represent less than 1% of blood cells but have a critical role in producing antibodies and identifying and disposing of foreign substances. Monocytes and lymphocytes are two particular types of leukocytes that have been implicated in the early stages of atherosclerosis and support the current view of atherosclerosis as a chronic inflammatory disease (Ross, 1999). The third major category of blood cells, thrombocytes or platelets, represents approximately 5% of blood cells. Thrombocytes interact with the protein fibrinogen to form fibrin, a mesh that traps cells to aid in the healing process. Finally, the plasma consists of approximately 90% water, 8% plasma proteins, 1% inorganic substances, and 1% emulsified fat. Blood plasma comprises approximately 20% of the entire extracellular fluid of the body.

Of central importance in the cardiovascular system, the heart propels blood through the systemic and pulmonary arteries and receives it from the systemic and pulmonary veins. In the normal heart, during the diastolic phase of the cardiac cycle, blood entering the atria flows into the ventricles as the ventricles relax and pressures fall below atrial pressures. Blood flowing from the right atria passes through the tricuspid valve into the right ventricle, while blood travels from the left atria to the left ventricle through the mitral valve. During the systolic phase of the cardiac cycle, the rising pressure in the contracting left ventricle exceeds aortic pressure and blood is ejected from the left ventricle through the aortic valve into the ascending aorta. Simultaneously, once the rising right ventricular pressure exceeds the main pulmonary artery pressure, blood flows through the pulmonary valve into the pulmonary arteries. Blood fills the right atria from the superior and inferior vena cava and the left atria from the pulmonary veins as the blood exiting the atria during diastole reduces atrial pressure relative to the venous filling pressure. The cardiac cycle, once complete, repeats itself again, as it will another 35 million times each year for the average adult. A useful description of the relationship between ventricular pressure and flow during the cardiac cycle, the pressure-volume loop, is shown in Figure 1. Clearly, changes in left ventricular volume during ejection directly correspond to the aortic flow. The area inside the left ventricular pressure–volume loop corresponds to the work performed by the ventricle on the blood. As discussed in the following section, lumped parameter models of the heart are often developed with the aim of replicating the pressure–volume loop under a range of physiologic states.

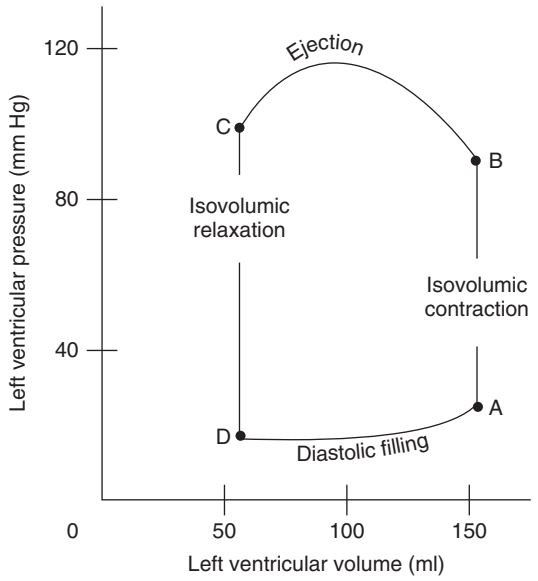

Figure 1. Left ventricular pressure–volume loop. The systolic phase of the cardiac cycle starts with isovolumic contraction (A–B) followed by ejection (B–C). Diastole begins ith isovolumic relaxation (C–D) followed by diastolic filling (D–A).

The final three key elements of all closed circulatory systems are the distribution system (arteries), exchange system (capillaries), and collection system (veins). For the purposes of this chapter, we focus our attention on the arterial system, but note that consideration of blood flow in the capillary bed necessitates consideration of the cellular nature of blood, and models of venous blood flow need to incorporate the physics of flow in collapsible tubes subject to low venous pressures. Turning our attention to the arterial system, we note that, in fact, there are two arterial systems in the body, the systemic and pulmonary arteries. For normal children and adults, these systems are in series, and the volumetric flow through each system is the same. However, because of a higher vascular resistance, blood pressures are approximately six times higher in the systemic circulation compared to the pulmonary circulation. Both arterial systems are often described using fractal geometry, and while there is some debate as to whether different parts of the vascular system are truly fractal in nature, at the very least, the arterial (and venous) systems are space filling, branching continuously to ever smaller vessels until the level of the capillaries is reached. Descending the vascular tree, the cross-sectional area increases, resulting in a decrease in the resistance of the vascular bed as compared to an area-preserving branching network. Alternate approaches have been used to describe the branching patterns of arteries, ranging from symmetric and asymmetric binary fractal trees (Olufsen, 1999) to diameter-defined Strahler systems that accommodate branching systems with small side branches coming off a larger trunk as frequently seen in the arterial system (Kassab and Fung, 1995; Choy and Kassab, 2008; Spilker *et al.*, 2007). Regardless of the method for describing the vascular anatomy, the direct representation of all the vessels from the major arteries to precapillary arterioles in a computational model is a daunting, and often intractable, task resulting in tens to hundreds of millions of vessels. We first consider methods that lump all these vessels into a small number of components and then describe methods to incorporate anatomically representative models of the entire vascular system.

3 ESTABLISHED METHODS IN BLOOD FLOW MODELING

3.1 Image-based modeling

Analysis and simulation of blood flow necessitates a combination of image analysis and model construction, boundary condition (BC) and material property selection, accurate solution of the governing equations, physiology models, and high-performance computing. Patient-specific cardiovascular simulations typically begin with 3D reconstruction of a portion of the vascular anatomy from CT or MRI image data and progress through stages of meshing, BC and parameter assignment, hemodynamic simulation, and flow analysis (Wilson *et al.*, 2001; Updegrove *et al.*, 2016; Taylor *et al.*, 1998b). This produces a wealth of data from which we aim to extract clinically relevant information to improve patient care. Since only a portion of a patient's anatomy can be included in the 3D model, both due to computational expense and limits of image resolution, BCs must be applied at inlets and outlets of the model to accurately represent the vascular network outside of the 3D domain, enabling physiologic representation of flow and pressure waveforms.

Patient-specific modeling requires construction of three-dimensional models of vascular anatomy derived directly from patient image data. The imaging modality is typically CT or MRI data, though ultrasound and angiography data can provide an attractive alternative. Image data is typically segmented using 2D or 3D level set or thresholding methods. Available packages for model construction are the open source packages SimVascular (www.simvascular.org), CRIMSON (www.crimson.software), and ITK-SNAP or commercial packages such as Mimics (Materialise, Leuven, Belgium) (Updegrove *et al.*, 2016). The model construction process typically employs a four-step process: (i) creation of centerline vessel paths, (ii) 2D segmentation of the lumen of each vessel, (iii) lofting segmentations to create

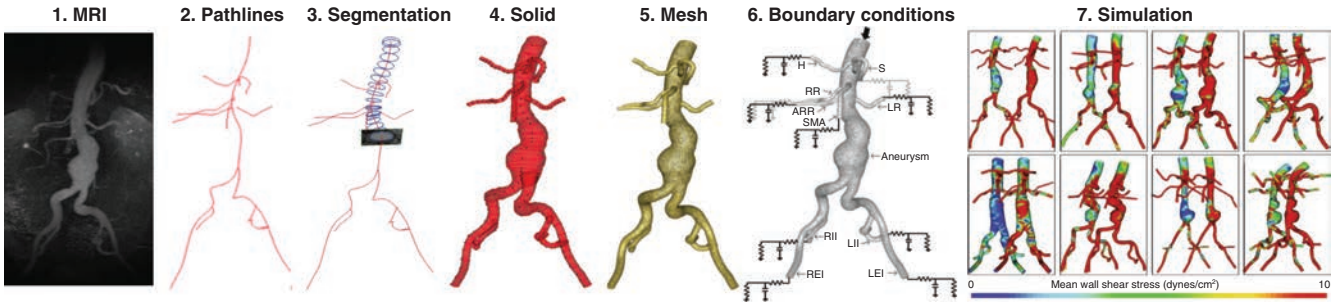

Figure 2. The typical steps in the patient-specific modeling process include (from left to right): importing medical image data, construction of centerline paths and segmentations, three-dimensional model construction, unstructured mesh generation, assignment of physiologic boundary conditions, and finite-element flow simulation to extract quantities of clinical interest. (Reproduced with permission from Les *et al.*, 2010. © Biomedical Engineering Society, 2010.)

a 3D model with multiple branches, and (iv) unstructured mesh generation. The steps of the typical patient-specific modeling process are shown in Figure 2. Image segmentation methods are a challenging component of the cardiovascular modeling process, often requiring extensive user intervention and manual segmentation to supplement automated methods. Recent efforts to improve automated segmentation algorithms have focused on machine learning algorithms and shape analysis and have also been extended to 3D segmentation methods using region growing and active contours (Merkow *et al.*, 2015). Continued advancements in these areas will be crucial to enable high-throughput processing of models for large patient cohorts in clinical studies.

3.2 Zero-dimensional methods

Perhaps the simplest model one can use to model blood flow in the cardiovascular system is a 0D lumped parameter method, which utilizes an analogy between fluid flow in the heart and vascular system and current flow in electric circuits to obtain systems of ordinary differential equations (ODEs) governing pressure and flow rate over time. In this method, pressure and flow rate replace voltage and current, resistors and inductors are used to represent the viscous and inertial properties of blood, and capacitors to represent elastic wall behavior (Westerhof *et al.*, 1969, 2009).

Using this analogy, some basic building blocks of a 0D lumped parameter network (LPN) can be defined as follows. Making the analogy of flow rate to current, and pressure drop to voltage, the relations for a resistor (R), capacitor (C), and inductor (L), with appropriate analogies to fluid dynamics, where ΔP is pressure drop and Q is flow rate, are as follows:

$$V = IR \Rightarrow \Delta P = QR \tag{1}$$

$$V = \frac{d}{dt}LI \Rightarrow \Delta P = \frac{d}{dt}LQ \tag{2}$$

$$I = \frac{d}{dt}CV \Rightarrow Q = \frac{d}{dt}CP \tag{3}$$

Making a rigid wall, Poiseuille flow assumption, the resistance of a section of blood vessel is

$$R = \frac{8\mu l}{\pi a^4} \tag{4}$$

where a is the vessel radius, μ viscosity, and l the vessel length, so that resistance is inversely propotional to the fourth power of the radius. These circuit building blocks can then be used to assemble networks of vessels and organs. At element junctions, conservation of mass is enforced following Kirchoff's law and continuity of pressure is assumed.

One of the most interesting applications of the lumped parameter method is in constructing a model of the heart that can reproduce pressure–volume data and cardiac function. In this approach, the contraction of the heart is modeled using time-varying capacitors and unidirectional flow through heart valves is modeled using diodes. The maximum pressure developed in the ventricles is directly related to the "afterload" posed by the vascular system. Here, simple lumped parameter models, such as the RCR circuit (where a relatively small upstream resistor is connected in series to a parallel arrangement of a capacitor and downstream resistor), have been used to model the effect of arterial compliance and a high resistance distal vascular bed on pressure and flow waveforms. This approach is particularly useful in developing in vitro mock circulatory systems for experimental flow studies (Kim *et al.*, 2009; Vukicevic *et al.*, 2013).

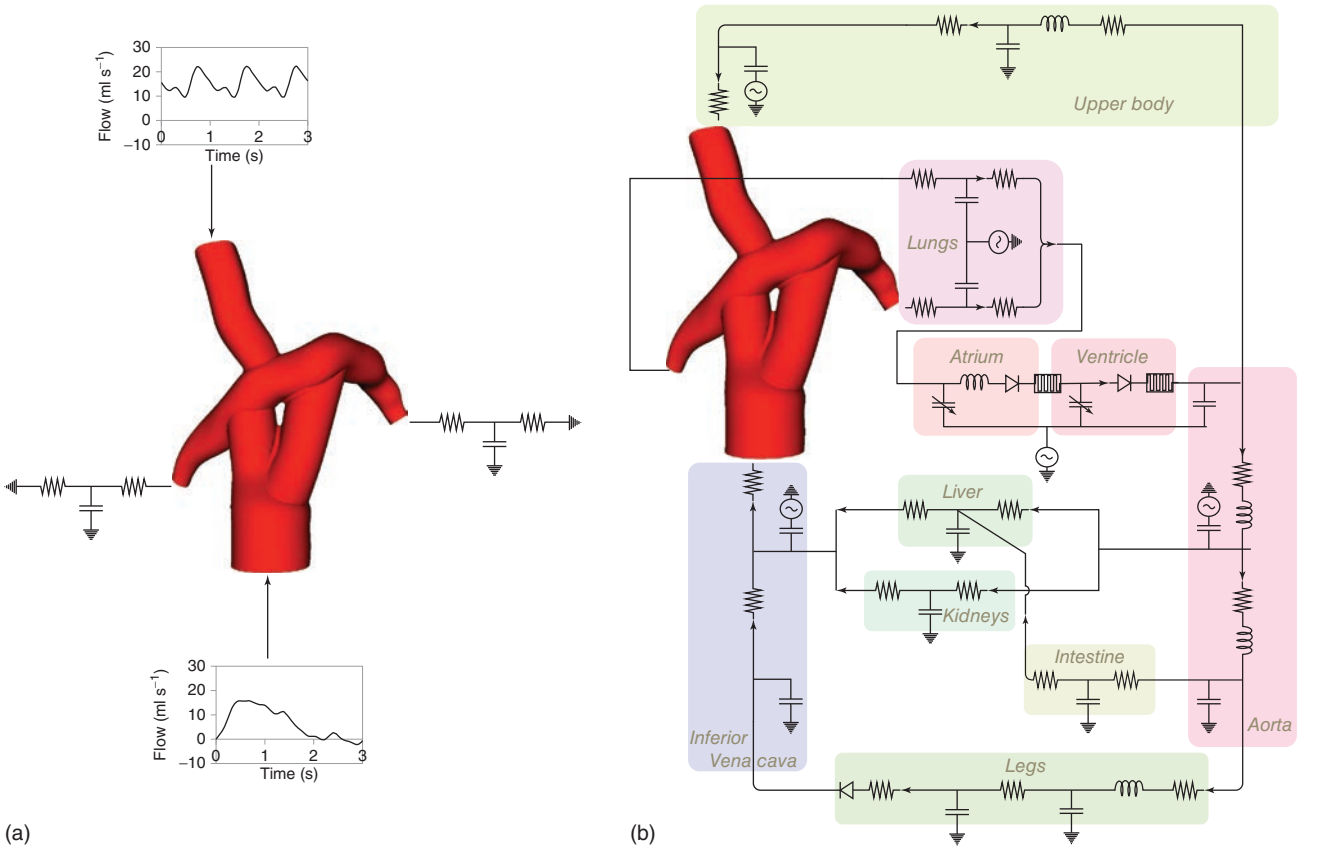

Figure 3. A patient-specific model of the Fontan surgery with a Y-graft configuration illustrating the use of open-loop (a) and closed-loop (b) boundary condition configurations for multiscale modeling.

In addition to cardiac models, lumped parameter models provide a surprisingly accurate representation of the closed-loop circulatory physiology. Lumped parameter models have been used to provide BCs for other analysis methods and are an essential component in efforts to develop "closed-loop" circulatory models (Esmaily-Moghadam *et al.*, 2013b; Lagana *et al.*, 2002; Sankaran *et al.*, 2012; Corsini *et al.*, 2011). The RCR (Windkessel) circuit is commonly adopted as an outlet BC to model the distal vasculature with one capacitor modeling vessel compliance and two resistors modeling proximal and distal pressure drops. Diodes and other specialized components may also be included to model heart valves and elastance of heart chambers. As some circuit components are time dependent, for example, due to the presence of inductors and capacitors, the circuit is represented by a set of time-dependent ODEs. Combining these equations produces a single ODE with order equal to the number of time-dependent components in the circuit. For simple circuits with low-order ODE, an analytical solution can be obtained, as is the case with simple resistors, RCR (Windkessel) circuits, and coronary artery models, which are commonly used as outlet BCs in an open-loop configuration. Models can be expanded to a full closed-loop networks that can then be coupled to the 3D domain. A closed-loop lumped-parameter model has the advantage that the effects from the global circulation are fully coupled to influence the overall simulated physiology. Figure 3 shows an example of closed-loop and open-loop multiscale simulation setups. Two limitations of lumped parameter models are worth noting. First, since geometry is not explicitly defined, wave propagation effects are not incorporated in lumped parameter models. Second, the determination of model parameters is generally based on the behavior of the entire system or subsystem, not on first principles as in the case of methods that emanate from initial-boundary-value problems. As a result, changes to components of the system, for example, a single artery, or an entire vascular bed, are not easily modeled.

3.3 One-dimensional methods

Nonlinear and linear 1D methods can accurately describe pulse wave propagation phenomena in extensive vascular networks while keeping the computational cost down. 1D methods are based on the assumptions that the dominant component of blood flow velocity is oriented along the vessel axis and that pressure can be assumed constant over the cross section of the vessel. For the flow of a Newtonian fluid in a deforming, impermeable, elastic domain, these equations consist of the following: (i) a continuity equation, (ii) a single axial momentum balance equation, and (iii) a constitutive equation (also known as tube law), together with suitable initial and BCs. Originally developed by Hughes and Lubliner (1973), the most commonly used form of the nonlinear continuity and momentum balance 1D equations of blood flow is as follows (Sherwin *et al.*, 2003; Peiró *et al.*, 2009):

$$\begin{cases} \dfrac{\partial A}{\partial t} + \dfrac{\partial (AU)}{\partial x} = 0 \\ \dfrac{\partial U}{\partial t} + U\dfrac{\partial U}{\partial x} + \dfrac{1}{\rho_\mathrm{f}}\dfrac{\partial P}{\partial x} = \dfrac{f}{\rho_\mathrm{f} A} \end{cases} \tag{5}$$

where x is the axial coordinate along the vessel, t the time, $A(x,t)$ the cross-sectional area of the lumen, $U(x,t)$ the axial blood flow velocity averaged over the cross section, $P(x,t)$ the blood pressure averaged over the cross section, ρ_f the density of blood assumed to be constant, and $f(x,t)$ the frictional force per unit length. These equations assume a value of one for the momentum correction factor in the convection acceleration term of equation (5), following the work of Stergiopulos *et al.* (1992).

Often, the velocity profile is assumed to be constant in shape and axisymmetric. The axial velocity (u) can be described by a polynomial:

$$u(x,\xi,t) = U(x,t)\frac{\zeta+2}{\zeta}\left[1-\left(\frac{\xi}{r}\right)^{\zeta}\right] \tag{6}$$

where $r(x,t)$ is the lumen radius, ξ the radial coordinate, and ζ the polynomial order. $\zeta = 9$ has been shown to provide a good compromise fit to time-resolved experimental data (Smith *et al.*, 2002). If we consider an axisymmetric vessel, the frictional force per unit length yields $f(x,t) = 2\mu\pi r\frac{\partial u}{\partial \xi}|_{\xi=r}$. For the velocity profile given by equation (6), we have $f = -2(\zeta+2)\mu\pi U$ in which the local f is proportional to the local flow. Note that $\zeta = 2$ leads to the Poiseuille flow resistance $f = -8\mu\pi U$. An explicit algebraic relationship between P and A (or *tube law*) is also required to close eqaution (5) and account for the FSI of the problem. In general, we have $P = \mathcal{A}(A(x,t);x,t)$, where the function $\mathcal{A}$ depends on the model used to describe the dynamics of the arterial wall.

In the 1D model, each cross section is assumed to deform axisymmetrically and independently from the others. A relationship between circumferential hoop stress, T_θ, and radial displacement can then be invoked: displacement can then be invoked:

$$T_\theta = \frac{E}{1-\nu^2}\frac{r-r_\mathrm{d}}{r_\mathrm{d}} \tag{7}$$

where r_d is the radius at diastolic pressure (P_d). Applying Laplace's law, $T_\theta = (P-P_\mathrm{d})r/h$, and assuming that $1/r$ can be approximated by $1/r_\mathrm{d}$, we obtain the following constitutive equation (Alastruey *et al.*, 2011):

$$\begin{aligned} P &= P_\mathrm{d} + \frac{4}{3}Eh\frac{r-r_\mathrm{d}}{(r_\mathrm{d})^2} = P_\mathrm{d} + \frac{\beta}{A_\mathrm{d}}(\sqrt{A}-\sqrt{A_\mathrm{d}}), \\ \beta &= \frac{4}{3}\sqrt{\pi}Eh \end{aligned} \tag{8}$$

where $A_\mathrm{d}(x)$ is the luminal area at diastolic pressure. In equation (8), both E and h are functions of the position x. The pulse wave speed $c(x,t)$ is related to A through

$$c = \sqrt{\frac{\beta}{2\rho_\mathrm{f}A_\mathrm{d}}}A^{1/4} \tag{9}$$

The initial area A_0 is calculated by replacing $P = 0$ and $A = A_0$ in equation (8), which leads to

$$A_0 = A_\mathrm{d}\left(1-\sqrt{A_\mathrm{d}}\frac{P_\mathrm{d}}{\beta}\right)^2 \tag{10}$$

When solving 1D simulations in a network of vessels, one must involve matching conditions at bifurcations by taking into account the correct propagation of the characteristic information and neglecting energy losses (Alastruey *et al.*, 2008). Nonlinear 1D formulations naturally account for nonlinear advective losses in the flow and are able to appropriately describe pulse wave propagation in the cardiovascular system. These formulations are particularly well suited for modeling blood flow in the larger arteries. In addition to accounting for pulse wave propagation, they also enable a simple framework to utilize viscoelastic constitutive models (Valdez-Jasso *et al.*, 2011; Raghu *et al.*, 2011), a trait of recognized importance in the behavior of the arterial system (Holenstein *et al.*, 1980).

The 1D theory, due to its low computational cost, has been applied to model hemodynamics in large arterial networks (Reymond *et al.*, 2009; Blanco *et al.*, 2015) and, in particular, to understand pulse wave propagation in human and animal circulations (Matthys *et al.*, 2007; Alastruey *et al.*, 2011). Recently, formulations have been derived that enable a more accurate characterization of quantities such as wall shear stress (WSS), by releasing the common assumption in 1D

methods in which velocity and flow waveforms are in phase (Bessems *et al.*, 2007). Furthermore, studies have confirmed that 1D simulations produce flows and pressure waveforms that compare well with those obtained with 3D formulations, in both idealized (Xiao *et al.*, 2014) and even subject-specific geometries (Alastruey *et al.*, 2016).

However, 1D methods are not well suited to study situations in which the flow is complex due to curvature, branching, and stenoses. Here, the axisymmetric assumption, fundamental to any 1D models, simply breaks down. There have been attempts to address this limitation by developing empirically derived losses to model the effects of stenoses (Seeley and Young, 1976; Young and Tsai, 1973; Stergiopulos *et al.*, 1992; Olufsen, 1999). However, these approaches introduce ad hoc parameters that must be calibrated for each specific problem. Therefore, in situations in which the flow is complex, as is commonly the case in disease conditions (e.g., stenosis, aneurysms, fistulas, and shunts), or in situations in which a medical device is deployed in the system, 3D methods must be utilized in order to describe such flows.

3.4 Three-dimensional methods

Although the suspension fluid, plasma, is largely composed of water, the large concentration of cells results in a non-Newtonian rheological behavior for whole blood. Specifically, blood exhibits a shear-thinning behavior where the viscosity at any shear rate increases with an increased percentage of cells (Fung, 1984). Despite this, it is generally accepted that blood flow in the large vessels can be represented as an incompressible fluid whose constitutive behavior is usually approximated by a Newtonian model. Arterial blood flow has been traditionally represented using the Incompressible Navier–Stokes equations in a fixed Eulerian frame of reference. However, blood velocity and pressure fields can be greatly influenced by the motion of external or internal vascular structures, such as the contracting cardiac muscle, moving heart valves, or deforming large arteries. In these situations, one must characterize the mechanical behavior of the moving vascular structure and its interactions with the blood flow. Depending on whether the deformability of the vascular structures is considered or not, one must choose between adopting a rigid wall and an FSI formulation. Rigid wall analyses are significantly less computationally expensive and provide useful information when the goal is to characterize transport, WSS and derivative quantities, and overall flow and pressure. In contrast, when studying processes in which the interaction between blood and vascular structure is important, such as hypertension, aneurysms, or a variety of device–vessel interactions, FSI formulations must be utilized.

3.4.1 Rigid wall formulations

The governing equations for the three-dimensional theory of blood flow under the assumptions of an incompressible, homogeneous, Newtonian fluid flow in a fixed Eulerian frame consist of the Navier–Stokes equations and suitable initial and BCs:

$$\begin{aligned} \rho(\dot{\boldsymbol{v}} + \boldsymbol{v}\cdot\nabla\,\boldsymbol{v}) &= -\nabla\, p + \nabla\,\cdot\boldsymbol{\tau}_{\mathrm{f}} + \boldsymbol{b} && \text{in } \Omega^{\mathrm{f}} \\ \nabla\cdot\boldsymbol{v} &= 0 && \text{in } \Omega^{\mathrm{f}} \\ \boldsymbol{v}(\boldsymbol{x}, t=0) &= \boldsymbol{v}_0 && \text{in } \Omega^{\mathrm{f}} \\ \boldsymbol{v} &= \boldsymbol{g} && \text{on } \Gamma_{\mathrm{g}} \\ (-p\boldsymbol{I} + \boldsymbol{\tau}_{\mathrm{f}})\cdot\boldsymbol{n} &= \boldsymbol{h} && \text{on } \Gamma_{\mathrm{h}} \end{aligned} \tag{11}$$

where Ω^{f} denotes the domain where the flow takes place, $\boldsymbol{v}$ the fluid velocity, p the pressure, $\boldsymbol{b}$ a body force, $\boldsymbol{n}$ a boundary unit normal, ρ the density, and $\boldsymbol{\tau}_{\mathrm{f}} = \mu(\nabla\,\boldsymbol{v} + (\nabla\,\boldsymbol{v})^{\mathrm{T}})$ the viscous stress tensor for a Newtonian fluid. Γ_{g} and Γ_{h} are the Dirichlet and Neumann portions of the boundary, respectively.

These equations are solved numerically using either finite elements or finite volume methods. In the past two decades, the number of contributions to the field in which the 3D Navier–Stokes were solved to simulate hemodynamic problems can be counted by the thousands, in areas ranging from disease research, to medical device design and performance evaluation, to noninvasive diagnostics, and even virtual surgical planning. Commercial packages have made these formulations readily accessible to a wide range of users. However, these packages often limit the user in terms of both proper mesh refinement strategies and, most importantly, the ability to include sophisticated inflow and outflow BCs that can meaningfully represent the hemodynamics of the system at hand (Section 3.5).

Perktold in the late 1980s and early 1990s was a pioneer in the use of computational methods to solve the 3D Navier–Stokes equations to represent blood flow in human arteries (Perktold and Hilbert, 1986; Perktold *et al.*, 1987, 1991a,b; Perktold and Peter, 1990). Taylor, Hughes and Zarins then pioneered the paradigm of "image-based" modeling, in which geometrical models of the vessels of interest are extracted from medical image data and computational methods used to solve the incompressible Navier–Stokes equations (Taylor *et al.*, 1996, 1998b).

The methods have been used successfully to study hemodynamics in abdominal aortic aneurysms (Les *et al.*, 2010; Tang *et al.*, 2006), the pulmonary arteries (Tang *et al.*, 2011), cerebral aneurysms (Cebral *et al.*, 2005a,b; Sforza *et al.*, 2009), the Fontan circulation (Marsden *et al.*, 2007, 2009), aortic coarctation (LaDisa *et al.*, 2011a,b; Coogan *et al.*, 2013), and aortic dissection (Dillon-Murphy *et al.*, 2016). Lagrangian analysis has been used to characterize coherent structures within cardiovascular flows (Shadden and Taylor,

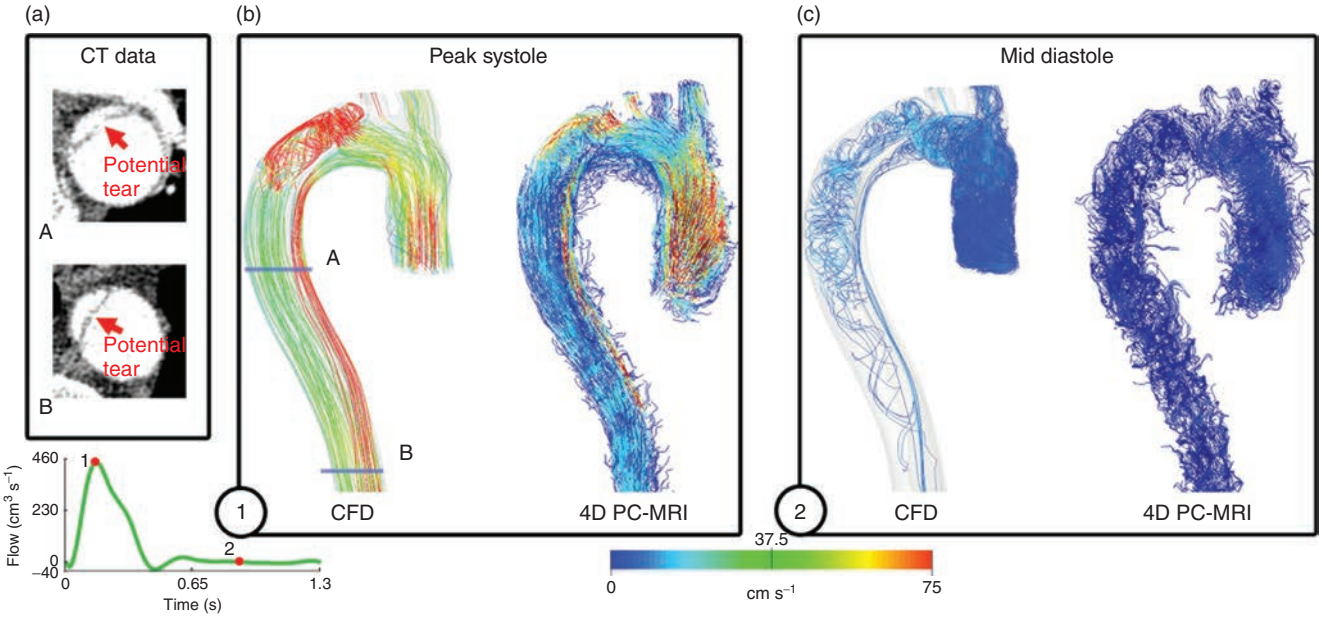

Figure 4. Comparison of CFD data and acquired 4D PC-MRI flow data at peak systole and mid-diastole in a patient with Type B aortic dissection. In aortic dissection, the aorta is divided into two different passages, a true lumen and a false lumen. Multiple communication tears may connect the two passages, creating a complex hemodynamic environment. (a) The computed tomography image data at two locations shows suspected connecting tears between the true and false lumina (Dillon-Murphy *et al.*, 2016). panels b and c compare CFD and 4D PC-MRI velocity patterns at peak systole and mid diastole, respectively. (Dillon-Murphy, https://link.springer.com/article/10.1007/s10237-015-0729-2. Used under CC BY 4.0 https://creativecommons.org/licenses/by/4.0/.)

2008). In summary, the development of advanced imaging modalities, with higher spatial and temporal resolution, and even time-resolved volumetric velocity information (e.g., 4D PC-MRI Markl *et al.*, 2007), make for a closer integration between medical data and computation of hemodynamics (Figure 4).

Recently, the field has witnessed the first commercial application of 3D computational methods for blood flow. Heartflow, Inc. received FDA approval in 2014 for a workflow in which the severity of coronary artery disease can be assessed using computed tomography data to reconstruct the main vessels of the coronary tree of a patient, and computer simulations of blood and pressure (Taylor *et al.*, 2013) to estimate the so-called FFR_{CT} (fractional flow reserve), a normalized metric of pressure gradients through a stenotic vessel under conditions of maximum flow.

It is apparent that 3D methods for blood flow in rigid domains constructed from image data are in a very advanced stage of maturity. Provided that appropriate inflow and outflow BCs are specified via multiscale or multiresolution methods (Section 3.5) and that proper care is given to achieving mesh-independent solutions, these formulations have been widely effective in situations in which the goal is to characterize quantities such as pressure, pressure gradients, flow distributions, WSS and its derivatives, and transport.

3.4.2 *Fluid–structure interaction formulations*

Blood velocity and pressure fields can be greatly influenced by the motion of external or internal vascular structures, such as the contracting cardiac muscle, moving heart valves, or deforming large arteries of the body. In these situations, one must characterize the mechanical behavior of the moving vascular structure (usually in a Lagrangian frame of reference) and its interactions with the blood flow, defining an FSI problem. We next provide an overview of the different families of FSI methods that have been used to model cardiovascular FSI problems.

Arbitrary Lagrangian–Eulerian formulations. In the arbitrary Lagrangian–Eulerian (ALE) formulation (Hughes *et al.*, 1981; Le Tallec and Mouro, 2001), the Navier–Stokes equations are written in a moving reference frame that follows the motion set by the vascular structure (Figure 5). At this interface, kinematic (continuity of velocities) and dynamic (equilibrium of tractions) compatibility conditions must be satisfied between fluid and structure. In ALE formulations, the motion of computational grid in which the flow problem is described is arbitrary and defined by a grid velocity $\boldsymbol{v}_G = (\frac{\partial \boldsymbol{x}}{\partial t})_{\chi}$. This velocity is defined by the Lagrangian motion of the vascular structure at the fluid–solid interface $\Gamma^s_{\boldsymbol{x}}$, but it needs to be propagated to all grid points

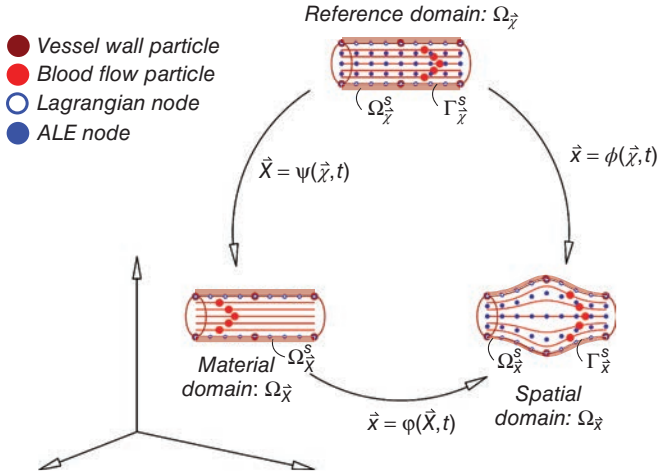

Figure 5. Different configurations used in the ALE formulation.

in the interior of the flow domain. In an ALE formulation, one must therefore solve the following three-field problem (Figure 5):

1. The Navier–Stokes equations of motion of a fluid in a moving spatial domain Ω_x, to represent the blood motion,

$$\begin{aligned} \rho\left(\frac{\partial \boldsymbol{v}}{\partial t}_{\chi} + (\boldsymbol{v} - \boldsymbol{v}_G)\cdot\nabla_{\boldsymbol{x}}\boldsymbol{v}\right) &= -\nabla_{\boldsymbol{x}} p \\ &\quad + \nabla_{\boldsymbol{x}}\cdot\boldsymbol{\tau}_{\mathrm{f}} + \boldsymbol{b} \quad \text{in } \Omega_{\boldsymbol{x}} \\ \nabla_{\boldsymbol{x}}\cdot\boldsymbol{v} &= 0 \qquad\qquad\quad \text{in } \Omega_{\boldsymbol{x}} \end{aligned} \tag{12}$$

2. The elastodynamics equations of motion of the vascular structure written in a Lagrangian frame of reference with respect to some initial configuration,

$$\rho_0^s\left(\frac{\partial \boldsymbol{v}}{\partial t}_{X} + \nabla_X(\boldsymbol{FS})\right) = \boldsymbol{b}_0 \quad \text{in} \quad \Omega_X^s \tag{13}$$

3. The motion of the computational grid for the blood flow domain, defined by an arbitrary mapping $\boldsymbol{x} = \boldsymbol{\phi}(\boldsymbol{\chi}, t)$ that matches the motion of the structure at the interface $\Gamma_{\boldsymbol{x}}^s$.

The ALE formulation is a boundary-fitting technique, in which the fluid–solid interface is accurately captured due to continuous updating of the fluid grid. However, in problems with large deformations in the vascular structure, ALE formulations may be time consuming. Modular (e.g., staggered) and nonmodular (e.g., monolithic) approaches for the solution of the coupled algebraic system resulting from the space–time discretization of the FSI problem have been proposed. Modular preconditioners allow for the use of independent, specialized fluid and structure solvers coupled via a relatively simple iterative scheme. These algorithms may exhibit poor convergence in cardiovascular problems, in which the density of the fluid ρ and the structure ρ^s are comparable. Nonmodular preconditioners require a more elaborated coupling between the fluid and solid solvers but result in faster, more stable algorithms.

ALE formulations were first used in cardiovascular applications by Perktold and Rappitsch (1995) and Prosi *et al.* (2004). More recently, Gerbeau *et al.* (2005), Gerbeau and Vidrascu (2003) studied hemodynamics in FSI models of cerebral aneurysms and carotid bifurcations, Bazilevs *et al.* (2006), Zhang *et al.* (2007) performed patient-specific FSI simulations using an isogeometric framework, and Wolters *et al.* (2005) and Scotti *et al.* (2005) investigated FSI in patient-specific abdominal aortic aneurysm models.

Immersed Boundary Method formulations. The immersed boundary method (IBM) was first introduced by Peskin (1972, 2003) in the context of finite differences. The IBM is a non-boundary-fitting formulation in which the structure was represented by a set of nonconforming, interconnected elastic boundary points embedded in the fluid domain, which is kept fixed throughout the computations. IBM formulations have been used in cardiovascular applications by Lemmon and Yoganathan (2000) to examine left ventricular dysfunction; Watton *et al.* (2007) to study prosthetic mitral valves; Griffith *et al.* (2009) to investigate natural and prosthetic heart valves; and Vigmond *et al.* (2008) to develop a whole heart electro-mechano-fluidic computational framework. On the microscales, the IBM has also been applied to modeling the interactions of red blood cells and plasma in the meso-circulation (Bagchi, 2007).

Closely related to the IBM, the fictitious domain method, first developed by Glowinski *et al.* (1997) in the context of finite elements, introduced Lagrange multipliers to constrain the motion of the fluid and the solid at the interface. Baaijens (2001) subsequently developed an extension suitable for slender structures and performed cardiovascular FSI simulations of the aortic valve (De Hart *et al.*, 2003, 2004). van de Vosse *et al.* (2003) and van Loon *et al.* (2003). also utilized a combination of ALE and fictitious domain methods to simulate dynamics of heart valves.

Coupled Momentum Method. Figueroa *et al.* (2006) developed a "coupled-momentum method" in which the elastodynamics equations are coupled with the fluid through a fictitious body force that drives the motion of the vessel wall, which is modeled as a thin-walled membrane. This monolithic method, coupled with multidomain formulations for inflow and outflow BCs (Vignon-Clementel *et al.*, 2006), enables FSI simulations with small increase in computational cost compared to rigid wall models (LaDisa *et al.*, 2011a,b; Coogan *et al.*, 2013). It is particularly well suited to study pulse wave propagation in complex 3D vascular models built

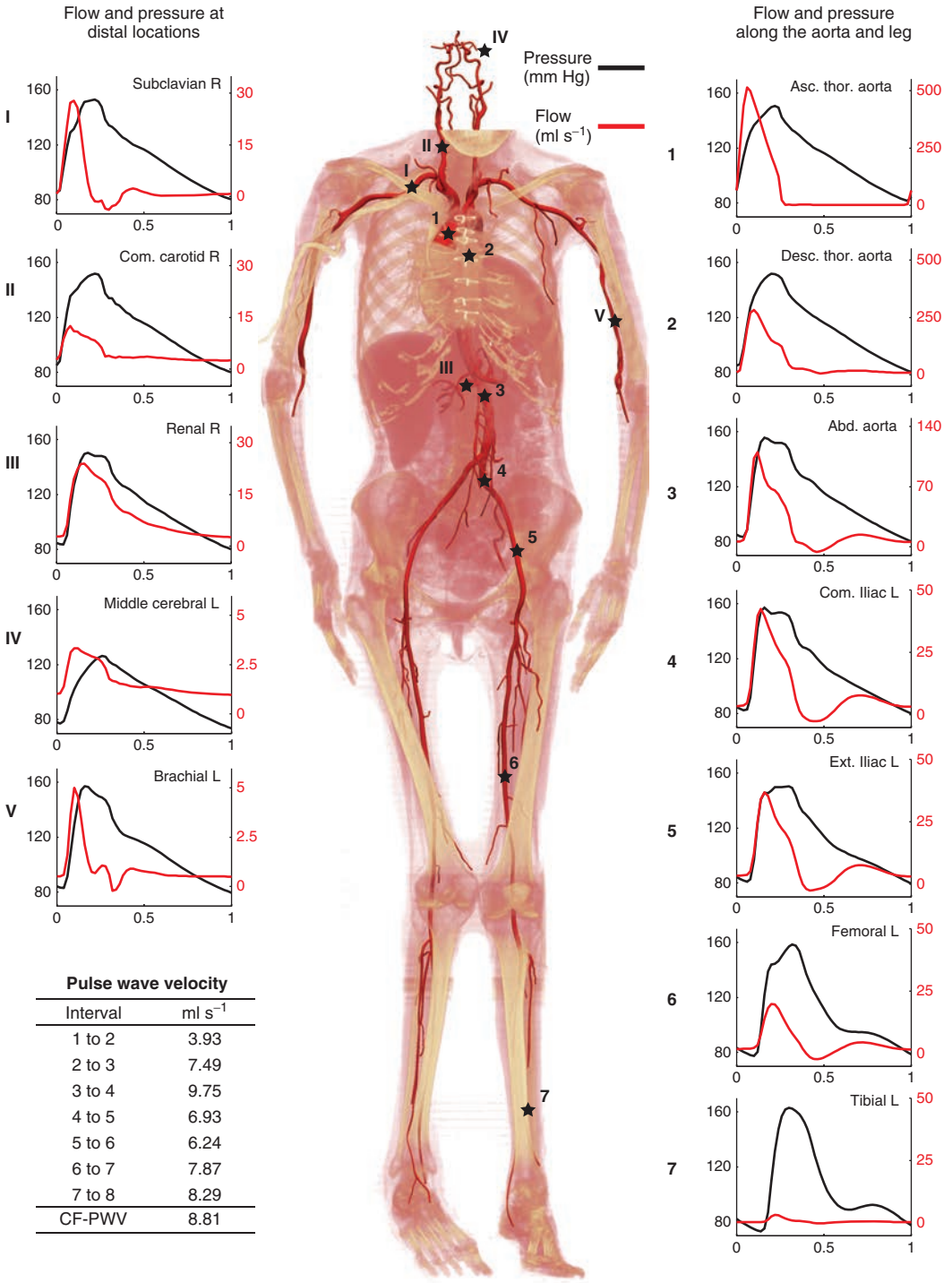

Pulse wave velocity

Interval	ml s^{-1}
1 to 2	3.93
2 to 3	7.49
3 to 4	9.75
4 to 5	6.93
5 to 6	6.24
6 to 7	7.87
7 to 8	8.29
CF-PWV	8.81

Figure 6. Pressure and flow waves at multiple sites in a full-body scale FSI model built from computed tomography. Table shows pulse wave velocity values obtained by measuring the time between the "foot" of the pressure waves at two sites. The calculated carotid-to-femoral pressure wave velocity (CF-PWV) is representative of typical values found in experimental measurements. (Reproduced with permission from Xiao *et al.*, 2013. © Elsevier, 2013.)

from both human (Xiao *et al.*, 2013) and animal image data (Cuomo *et al.*, 2015). Figure 6 shows 3D hemodynamics in a full-body vascular model consisting of the 84 largest arteries in the human. The model has spatially varying tissue properties that include higher compliance in the ascending aorta and smaller compliance in distal aorta and peripheral vessels. The model reproduces accurately regionally flow distributions, pressure and flow waveforms, and pulse wave velocity.

3.5 Multi-scale modeling

Because an image-based model is restricted to a certain region of the vascular anatomy and limited by image resolution to large and mid-sized vessels, it is crucial to employ multiscale modeling methods that capture organ-level responses of the circulation as well as resistance, impedance, and wave propagation effects of the distal vascular and capillary beds. In the following paragraphs, we describe recent developments toward modeling methods that capture these effects, primarily through the use of closed-loop lumped parameter networks and heart models.

The choice of BCs is of paramount importance in cardiovascular simulations, as the local flow dynamics are greatly influenced by conditions upstream and downstream of the 3D model. Numerous studies have demonstrated drastic differences in flow solutions with different BC choices, even with simple geometries, and particularly in models with multiple outlets (Vignon-Clementel *et al.*, 2006, 2010). Commonly used outlet BCs such as zero pressure or zero traction, while easiest to implement, are well known to lead to unrealistic solutions, in part because of their inability to capture physiologic levels of pressure. These methods should not be used for FSI problems where the wall deformation depends directly on the pressure level in the vessel. Vascular resistance in arterioles and capillaries is largely responsible for determining blood pressure levels in large arteries. The same vascular resistances are also responsible for regulating the distribution of blood flow to different regions of the body. A fluid dynamic simulation of large arteries, without consideration of the smaller downstream vessels, neglects these important effects.

A typical choice of inlet BC is to impose a prescribed pressure or flow waveform. Typical choices for outlets are zero pressure or zero traction conditions, resistance or impedance conditions, reduced order models which can be open or closed loop, or reduced order 1D wave propagation equations (Vignon-Clementel *et al.*, 2006, 2010; Formaggia *et al.*, 2003). A closed-loop approach can also be taken, in which all boundaries of the 3D model are coupled to a lumped parameter network. These BCs are imposed via a Dirichlet condition

$$\boldsymbol{u} = \boldsymbol{g},\ \boldsymbol{x} \in \Gamma_{\mathrm{g}} \tag{14}$$

or a Neumann condition

$$\boldsymbol{T} \cdot \boldsymbol{n} = \boldsymbol{h},\ \boldsymbol{x} \in \Gamma_{\mathrm{h}} \tag{15}$$

in which Γ_{g} and Γ_{h} denote Dirichlet and Neumann boundaries, respectively.

Note that $\boldsymbol{g}$ and $\boldsymbol{h}$ are a prescribed function of $\boldsymbol{x}$ and t for uncoupled BCs (e.g., zero traction), whereas they are also a function of $\boldsymbol{u}$ and p for complex reduced order models (e.g., closed-loop heart models).

Here, we discuss BCs coming from closed-loop lumped parameter networks. To capture the interaction between the local 3D domain and the global circulation, the 3D Navier–Stokes solver must be coupled to a reduced order LPN model. In a closed-loop configuration, the 3D domain inflow is extracted from the 0D domain solution, incorporating the responses of the heart and global physiology to altered flow conditions at the 3D–0D interface. In a closed-loop scenario, the 3D domain presents itself to the 0D model as a set of time-varying resistance, inductance, and capacitance (in the case of deformable wall simulation), which are functions of the 3D domain hemodynamics. The 0D model behavior is affected by this 3D model behavior and thus provides BCs that are fully coupled to the 3D domain, forming a complete feedback loop.

Closed-loop multiscale models have been particularly useful in modeling coronary flows, as well as complex surgeries in pediatric cardiology applications (Migliavacca *et al.*, 2003; Kung *et al.*, 2013; Sankaran *et al.*, 2012). For example, the effects of a surgical shunt in single ventricle patients can be investigated using such a model, which enables considerations of how the shunt resistance influences the balance of blood flow through various pathways in light of systemic resistances and heart behavior (Esmaily-Moghadam *et al.*, 2012). After defining the physics of the 3D and reduced-order domains, the coupled system must be solved by a numerical method that is both stable and modular. A summary of recent methods for stable and efficient coupling can be found in Marsden and Esmaily-Moghadam (2015).

Depending on the complexity and order of the ODE network governing the LPN, one may use either a monolithic or a coupled approach for solution of the 0D–3D coupled system. A monolithic approach can be used when the analytical solution of the ODE of 0D model is known and can be implemented directly in the numerical solver

and the entire problem solved simultaneously. The monolithic approach is now widely accepted with details described in foundational work by Vignon-Clementel *et al.* (2006) and is best suited to simple models, at most containing few time-dependent components, such as resistance and RCR circuits.

For more complex circuit networks, obtaining the analytical solution of a high-order nonlinear ODE is not practical, and the system must be solved numerically to obtain the Dirichlet-to-Neumann relationship. Use of the monolithic approach is no longer practical in this case, and partitioned approaches have been introduced by several groups Esmaily-Moghadam *et al*. (2013b), Ismail *et al.* (2013), and Kuprat *et al.* (2013). The key concept of the partitioned approach is to have a separate solver for the 0D domain that is coupled to the 3D solver through a well-defined interface. Numerical solution of the ODEs in the 0D solver, for example, with a Runge–Kutta time-stepping scheme, enables simulation of circuits with multiple time-dependent and nonlinear components and multiple organ blocks.

Recent studies have also addressed issues of numerical divergence due to back flow, as well as specialized preconditioners (Esmaily-Moghadam *et al.*, 2011, 2013a). While recent work has largely focused on 0D LPN models as the choice of reduced-order model, we note that multiscale modeling methods can be extended to 1D models by replacing the ODE governing the 0D model with partial differential equations governing the 1D model, while keeping the coupling scheme unchanged.

4 NOVEL COMPUTATIONAL TOOLS

4.1 Tissue growth and remodeling

Blood vessels exhibit remarkable ability to adapt throughout life adaptations in development and aging; to injury such as in wound healing and vasospasm; in disease, such as atherosclerosis and aneurysms; and lastly, adaptations to chronic increase in flow in endurance training, or to hypertension. These adaptations result in changes in vessel shape and material properties and depend on an array of factors such as gene pathways, biochemical processes in the vessel wall, and, as numerous findings over the past few decades indicate, the mechanical environment of the vessel. Many observations at the subcellular, cellular, and even cell matrix levels point to the existence of a "preferred" or "homeostatic" mechanical state across multiple space and time scales. Thus, it is thought that vascular G&R happens in response to a significant alteration of the homeostatic state of a vessel (Humphrey, 2008). Changes in the shape and mechanical properties of blood vessels are ultimately related to changes in its constituents: resident cells (smooth muscle and endothelial cells) and the extracellular matrix. The main remodeling agents in the vessel wall are the endothelial cells, vascular smooth muscle cells, and fibroblasts.

From a computational standpoint, two main methodologies have been proposed to study cardiovascular tissue G&R: a kinematic growth approach (Taber, 1998; Rachev, 2000) and a constrained mixture approach (Humphrey and Rajagopal, 2002; Watton *et al.*, 2004; Kuhl and Holzapfel, 2007). Kinematic growth formulations model the G&R without representing the underlying biochemomechanical mechanisms modulating growth. On the other hand, constrained mixture models incorporate the response of smooth muscle and collagen fibers to changes in mechanical loading (or potentially other biochemical stimuli). Each constituent can be produced and removed over time. The total mass of the mixture $M(\tau)$ at any given time $\tau \in [0, s]$ is given by a balance of production and survival functions (Baek *et al.*, 2006):

$$M(s) = \sum_i M^i(s) = \frac{1}{J(s)} \sum_i \left\{ M^i(0) Q^i(s) + \int_0^s m^i(\tau) q^i(s-\tau) J(\tau) d\tau \right\} \quad (16)$$

where $J(\tau)$ is the determinant of the deformation gradient $\boldsymbol{F}(\tau)$, $Q^i(s)$ the fraction of the ith constituent that was present at time 0 and still remains at time s, $m^i(\tau)$ the true rate of production of the ith constituent at time τ per unit area, and $q^i(s-\tau)$ its survival function, that is, the fraction of constituent i produced at time τ that remains at time s. The mass fractions of each constituent i $\phi^i(s)$ ($i =$ elastin, collagen$_1$, collagen$_2$, etc.) are given by

$$\phi^i(s) = \frac{M^i(s)}{M(s)} \quad \text{such that} \quad \sum_i \phi^i(s) = 1 \qquad \forall\, s \quad (17)$$

For an elastic body, the Cauchy stress $\boldsymbol{T}$ for the mixture can be given by sum of passive and active strain energy function contributions:

$$\boldsymbol{T}(s) = \frac{2}{J(s)} \boldsymbol{F}(s) \frac{\partial w_R(s)}{\partial \boldsymbol{C}(s)} \boldsymbol{F}(s)^T + \boldsymbol{T}_{(\text{act})}(s) \quad (18)$$

where $\boldsymbol{C} = \boldsymbol{F}^T \boldsymbol{F}$. The passive contribution to strain energy of the mixture per unit reference area w_R is defined as the sum of the energy stored in the elastin-dominated amorphous matrix and the multiple families of collagen, namely

$$w_R(s) = w_R^e(s) + \sum_k w_R^k(s) \quad (19)$$

The strain energy for the elastin-dominated matrix is typically assumed to be neo-Hookean. For collagen, the form of the strain energy function is assumed identical for all fiber families and is typically given by an exponential Holzapfel form (Holzapfel *et al.*, 2000). This is an illustrative example of a linearized form for the rate of mass production (Figueroa *et al.*, 2009):

$$m^k(s) = \frac{M(s)}{M(0)}(k_\sigma(\sigma^k(s) - \sigma^h) + k_\tau(\tau_w(s) - \tau_w^h) + m^k_{\text{basal}}) \tag{20}$$

where k_σ and k_τ are scalar parameters that control the stress-mediated G&R and m^k_{basal} is a basal rate of mass production for the kth fiber family. At the homeostatic state, therefore, the production rate follows the basal rate.

In Figueroa *et al.* (2009), Humphrey, Figueroa and colleagues developed a "fluid-solid-growth" (FSG) formulation in which the hemodynamic forces acting during the cardiac cycle pin an FSI simulation provide the loads for the vascular G&R formulation, defined on a timescale of weeks to months, which in turn provides the updated geometry and material properties for the hemodynamic simulation. This FSG framework was used to study the long-term evolution of a basilar artery aneurysm under different mechanical stimuli.

4.2 Parameter estimation and uncertainty quantification

4.2.1 Parameter estimation via filtering techniques

A primary challenge in constructing truly patient-specific hemodynamic models is the calibration of numerous parameters required to define both the mechanical properties of the vascular model (e.g., distribution of stiffness and perivascular tissue support) and in the inflow and outflow BCs so that the numerical predictions are consistent with clinical data. For 3D computational models, the high cost of a single forward simulation necessitates an efficient parameter estimation strategy that minimizes the number of model evaluations.

While information on flow and wall motion can be readily obtained from magnetic resonance imaging and computed tomography, reliable information on pressure can only be obtained via invasive catheterization. Lack of pressure data thus hinders knowledge of vascular stiffness and resistance. Typically, estimation of stiffness and resistance is done iteratively using traditional optimization approaches. This step is the most computationally expensive.

Traditional approaches for parameter estimation relied on defining a cost function constructed from the difference between data and simulation results, and performing classic optimization. This approach is quite expensive and is not particularly well suited for time-dependent problems.

Recently, data assimilation strategies based on Kalman filter theory (Julier *et al.*, 2000), in particular *reduced-order unscented Kalman filter* (ROUKF) formulations, have been used to estimate parameters in a number of cardiovascular and cardiac electrophysiology applications (Chapelle *et al.*, 2013; Marchesseau *et al.*, 2013; Xi *et al.*, 2011; Moireau *et al.*, 2012) in patient-specific vascular models. Unlike classic optimization, the Kalman filter is a sequential approach well suited to handle dynamical systems in which time-resolved measurements (data) are available. Given an evolution equation

$$\dot{X} = A(X) \tag{21}$$

where X is the state and A a model operator (e.g., Navier–Stokes), the Kalman filter adds a correction $K(Z - H(X))$, where $Z - H(X)$ is the difference between a measurement Z and a model prediction $H(X)$ (i.e., an innovation), and K is a gain operator. In addition to *parameter estimation*, the Kalman filter has perhaps a more interesting application in *model refinement*: indeed, the evolution equation

$$\dot{X} = A(X) + K(Z - H(X)) \tag{22}$$

can be seen as a balance between model (which might be fundamentally inadequate) and gain-regulated data. This framework enables the assessment of the suitability of a given model by identifying situations in which the estimated model parameters do not converge to steady values.

These techniques, albeit expensive (e.g., in the ROUKF, one must run $p + 1$ forward problem simulations to estimate p parameters), could make the process of parameter estimation completely automatic and operator independent, a highly critical feature in order to facilitate clinical translation of computational tools.

4.2.2 Uncertainty quantification

The adoption of simulation tools to predict surgical outcomes is increasingly leading to questions about the variability of these predictions in the presence of uncertainty associated with the input clinical data. A pitfall of current simulation methods is that they often fail to acknowledge or quantify the numerous sources of uncertainty involved in the clinical data assimilation and modeling process. As simulation data are increasingly incorporated into disease research, clinical trials, and the FDA approval process, there is a pressing need to establish strict guidelines for assessing the impact of uncertainty on simulation predictions.

A typical CV simulation is a multistep process consisting of 3D model reconstruction from medical image data, mesh

generation, tuning BCs to match physiologic and clinical data, flow simulation, and feedback to clinicians. This process involves numerous sources of uncertainty. Uncertainties stem from assimilation of clinical measurements (heart rate and blood pressure), echocardiography data (stroke volume, ejection fraction, and cardiac output), phase contrast and other MRI data, and cardiac catheterization data. Additional uncertainties stem from vessel-wall material properties and physiologic data. Noise, artifacts, and limited temporal and spatial resolution in CT and MRI image data also lead to uncertainty in the image segmentation process. These input uncertainties propagate nonlinearly through the modeling process, resulting in predictions that should be reported with associated statistics and confidence intervals on a patient-specific basis.

Solver performance is of utmost importance when performing optimization and UQ, both of which require running numerous simulations either in parallel or in succession. As CV simulations typically require multiple hours of run time on a large parallel cluster, Monte Carlo-like strategies quickly become computationally intractable for large problems. Maintaining tractability thus requires both optimized solver performance, for example, using specialized coupling and preconditioning methods, and efficient algorithms to limit the required number of function evaluations for convergence.

Recent work has applied stochastic collocation for UQ in computational fluid dynamics (CFD), providing probability density functions (PDFs) and confidence intervals on simulation outputs (Ghanem and Spanos, 1991; Xiu and Hesthaven, 2005; Babuška *et al.*, 2007). Collocation methods generally offer substantially better convergence than traditional Monte Carlo methods, are nonintrusive to implement, and are highly parallelizable. In the collocation scheme, stochastic space is approximated using mutually orthogonal interpolating functions and can then be queried at any point and PDF's can be constructed. This method is specifically designed for UQ in large-scale simulations, such as CFD simulations in complex geometries. Efficient application of UQ with stochastic collocation using sparse grids has been demonstrated for idealized and patient-specific cardiovascular models using a limited number of stochastic parameters (Sankaran and Marsden, 2010, 2011; Sankaran *et al.*, 2010). These studies employed Smolyak sparse grids to handle parametric uncertainty and quantify predictive uncertainty in terms of PDFs and confidence intervals (Babuška *et al.*, 2007; Xiu and Hesthaven, 2005; Ghanem and Kruger, 1996; Najm, 2009).

Recent work has also introduced methodologies for full propagation of uncertainty from clinical data to virtual surgery predictions in single-ventricle palliation, as illustrated in Figure 7. A recent study characterized the preoperative clinical uncertainty related to indirect wedge catheter measurements of mean pulmonary artery pressure and MRI-derived right pulmonary flow split. Inverse Bayesian estimation was then used to infer the distributions of boundary resistance modes, leading to the expected clinical PDFs and used stochastic collocation on sparse grids to propagate these BC distributions to the postoperative results. The effect of relieving the left pulmonary artery stenosis was also quantified both in terms of change in average results and associated confidence intervals (Schiavazzi *et al.*, 2015).

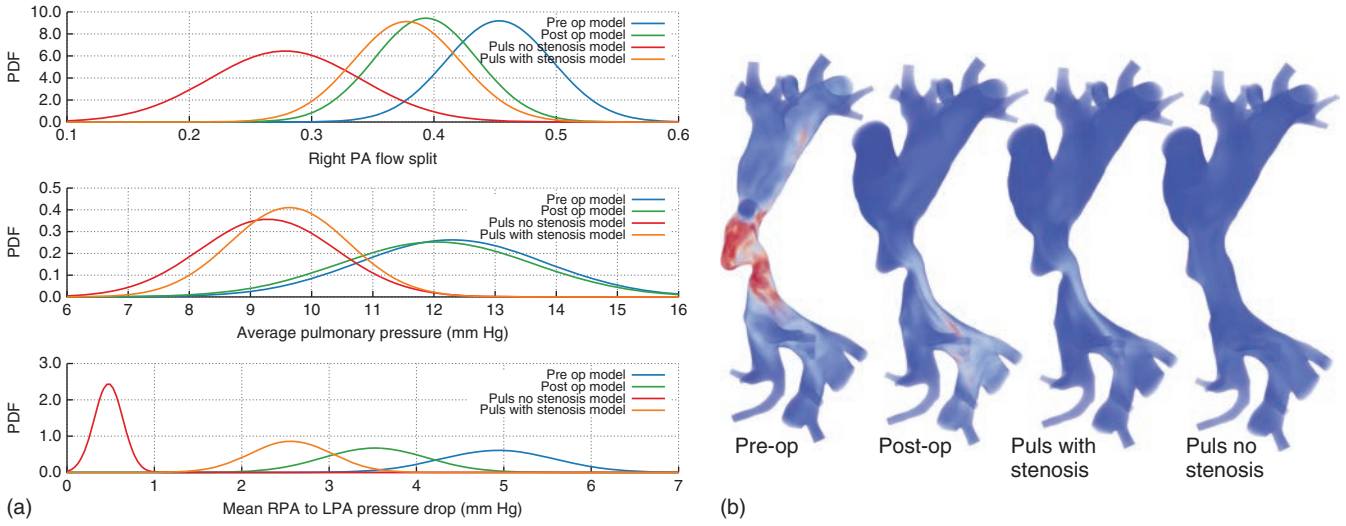

Figure 7. (a) Distribution of identified pre- and predicted postoperative clinical indicators for Stage II single-ventricle palliation surgery. (b) Standard deviation of local velocity results for pre- and postoperative models.

Figure 7 shows how the first two statistical moments of clinical quantities of interest have been affected by surgery, showing that postoperative flow split following surgical removal of left pulmonary stenosis becomes more difficult to predict due to increased sensitivity to variation in the BCs. Conversely, estimation of the pressure drop becomes more reliable. Figure 7 also shows the spatial distribution of variance in the velocity field for pre- and postoperative models. These methods can also be used to target-specific areas of data collection for model improvement. Recently, methods combining multiresolution representations and sparsity-promoting recovery algorithms have shown promise for reducing the number of model evaluations needed to compute accurate response statistics for multiscale CV models (Schiavazzi *et al.*, 2014).

4.3 Optimization

Coupling optimization to cardiovascular simulations has potential to improve surgical designs and enable individualized treatment planning. Optimization methods were first introduced in the field of cardiovascular modeling primarily in two-dimensional and steady flow problems (Agoshkov *et al.*, 2006a,b; Abraham *et al.*, 2005; Quarteroni and Rozza, 2003) and have recently been expanded to complex, three-dimensional, unsteady simulations (Esmaily-Moghadam *et al.*, 2012; Yang *et al.*, 2010). The coupling of optimization algorithms to blood flow simulations is particularly challenging because each cost function evaluation requires an unsteady, 3D solution of the Navier–Stokes equations on multiple processors. These evaluations are computationally expensive, and gradient information is often difficult to obtain.

Shape optimization can be used for virtual surgery design in which a patient-specific model is optimized to minimize a disease-related cost function derived from the flow field. Examples of surgery optimization include identifying optimal angles and radii for bypass grafts and finding the optimal shape of complex surgical connections for single ventricle heart patients (Yang *et al.*, 2013; Sankaran and Marsden, 2010). Optimization can also be used in the design of medical devices, including stents, ventricular assist devices, and coil placement for cerebral aneurysms (Long *et al.*, 2013; Gundert *et al.*, 2012a,b). Outside of shape optimization, one can also apply optimization in the setting of parameter identification for cardiovascular modeling. For example, optimization can be used to identify parameters in cardiovascular G&R or in determining material properties from medical image data for FSI (Sankaran *et al.*, 2013).

When choosing an optimization method, the primary distinction is between gradient-based and derivative-free methods. Factors contributing to this choice include the availability of cost function gradients, computational cost of the function evaluations, the level of noise and discontinuities in the function, complexity of implementation, the number of design parameters, convergence properties, efficiency, and scalability.

A general optimization problem may be formulated with linear bound constraints as follows:

$$\begin{aligned} &\text{minimize} \quad J(\mathbf{x}) \\ &\text{subject to} \quad \mathbf{x} \in \Omega \end{aligned} \tag{23}$$

where $J : \mathbb{R}^n \to \mathbb{R}$ is the cost function and $\mathbf{x}$ the vector of design parameters. The parameter space is defined by $\Omega = \{\mathbf{x} \in \mathbb{R}^n | \mathbf{l} \leq \mathbf{x} \leq \mathbf{u}\}$, where $\mathbf{l} \in \mathbb{R}^n$ is a vector of lower bounds on $\mathbf{x}$ and $\mathbf{u} \in \mathbb{R}^n$ a vector of upper bounds on $\mathbf{x}$. In a cardiovascular shape optimization problem, the function $J(\mathbf{x})$ depends on the solution of the Navier–Stokes equations, and the cost function value is computed in a post-processing step.

Derivative-free algorithms such as the surrogate management framework (SMF) have shown particular promise in cardiovasclar blood flow simulation due to their flexible implementation and ability to search globally in the parameter space. The main idea behind the SMF method is to increase efficiency using a surrogate function to "stand in" for an expensive function evaluation, while also benefiting from the convergence properties of pattern search methods (Audet and Dennis, 2004, 2006; Audet, 2004).

The SMF algorithm typically consists of a SEARCH step, employing a Kriging surrogate function for improved efficiency, together with a POLL step to guarantee convergence to a local minimum (Lophaven *et al.*, 2002; Simpson *et al.*, 1998). The exploratory SEARCH step uses the surrogate to select points that are likely to improve the cost function but is not strictly required for convergence. Convergence is guaranteed by the POLL step, in which points neighboring the current best point on the mesh are evaluated in a positive spanning set of directions to check if the current best point is a mesh local optimizer.

All points evaluated in either the SEARCH or POLL step of the SMF algorithm must lie on a mesh in the parameter space. The vectors defining the mesh directions must positively span $\mathbb{R}^n$ (Lewis and Torczon, 1996). If we define D as a matrix whose columns form a positive spanning set in $\mathbb{R}^n$, then the set of mesh points surrounding a point x are given by

$$M(x, \Delta) = \{x + \Delta D z : z \in \mathbb{N}^{n_D}\} \tag{24}$$

where Δ is the mesh size parameter and n_D the number of columns in D. A positive spanning set is simply the set

of positive linear combinations of the vectors making up the mesh directions (Davis, 1954). A set of $n+1$ POLL points are required to generate a positive basis, where n is the number of optimization parameters. Following the abovementioned definition, the mesh in SMF may be refined or coarsened by changing $\Delta > 0$, and the mesh may be rotated from one iteration to the next (Torczon, 1997).

Convergence is reached when a local minimizer on the mesh is found, and the mesh has been refined to the desired accuracy. Each time new data points are found in a SEARCH or POLL step, the data is added to the surrogate and it is updated. The steps in the algorithm are summarized below, where the set of points in the initial mesh is M_0, the mesh at iteration k is M_k, and the current best point is x_k.

1. SEARCH
   (a) Identify a finite set T_k of trial points on the mesh M_k.
   (b) Evaluate $J(z)$ for all trial points $z \in T_k \subset M_k$.
   (c) If for any trial point in T_k, $J(z) < J(x_k)$, a lower cost function value has been found, and the *SEARCH* is *successful*. Increment k and go back to (a).
   (d) Else, if no trial point in T_k improves the cost function, *SEARCH* is *unsuccessful*. Increment k and go to POLL.
2. POLL
   (a) Choose a set of positive spanning directions, and form the poll set X_k as the set of mesh points adjacent to x_k in these directions.
   (b) If $J(x_{\text{poll}}) < J(x_k)$ for any point $x_{\text{poll}} \in X_k$, then a lower cost function has been found and the *POLL* is *successful*. Increment k and go to SEARCH.
   (c) Else, if no point in X_k improves the cost function, *POLL is unsuccessful*.
      (i) If convergence criteria are satisfied, a converged solution has been found. STOP.
      (ii) Else if convergence criteria are not met, refine mesh. Increment k and go to SEARCH.

Because the method has distinct SEARCH and POLL steps, convergence theory for the SMF method reduces to convergence of pattern search methods. We refer the reader to the extensive literature summarizing the relevant mathematical convergence theory (Booker *et al.*, 1999; Serafini, 1998; Audet and Dennis, 2003; Torczon, 1997; Lewis and Torczon, 1999, 2000, 2002).

In the context of blood flow simulation, optimization has been used in the design of bypass grafts (Sankaran and Marsden, 2010) as well as surgeries for single ventricle heart patients. Optimization has uncovered links among graft position, cardiac output, and coronary oxygen delivery in the first stage of single ventricle repair, the Blalock–Taussig (BT) shunt (Esmaily-Moghadam *et al.*, 2012). In this chapter, optimization was performed on a 3D model of the aorta and pulmonary arteries, using the closed-loop-lumped parameter network discussed earlier. The graft geometry was parameterized and implanted into the model using automated scripts, and the 3D unsteady Navier–Stokes equations were solved in each function evaluation on a parallel architecture. A typical example of the implementation of shape optimization is shown in Figure 8.

5 CLINICAL APPLICATIONS

5.1 Pediatric cardiology

Multiscale modeling is of particular importance in pediatric cardiology due to the strong interactions between surgical methods and global physiology of the patient, including cardiac performance. Single ventricle heart defects are a particularly challenging class of congenital heart defects and present a complex physiology requiring three open-chest surgeries starting in the neonatal period and culminating with the Fontan surgery (Fontan and Baudet, 1971). First applied to single ventricle physiology by Dubini, Migliavacca, and Pennati, multiscale modeling extends standard simulation tools to predict not only local hemodynamics such as energy loss but also global quantities of clinical interest including ventricular work load, pressure volume loops, systemic and pulmonary pressure levels, and oxygen delivery (Leval and Dubini, 1996; Dubini *et al.*, 1996; Lagana *et al.*, 2002).

Early work on modeling single ventricle physiology focused on power loss as the primary metric of performance for comparing surgical geometries. Initial simulation studies demonstrated improved energy efficiency in Fontan surgical geometries with an offset between the superior and inferior vena cava (SVC and IVC), leading to widespread adoption of the offset concept in the surgical community (Migliavacca *et al.*, 2003; Dubini *et al.*, 1996). Subsequent studies went on to establish links between the geometry of the Fontan junction and hemodynamic performance (Migliavacca *et al.*, 2003; Petrossian *et al.*, 2006; Marsden *et al.*, 2007; Whitehead *et al.*, 2007; DeGroff, 2008; Soerensen *et al.*, 2007). Some have also suggested that high power loss is likely linked to poor clinical outcomes and high ventricular workloads and that energy reduction is of primary importance in surgical design (Ensley *et al.*, 2000a; Healy *et al.*, 2001; Ryu *et al.*, 2001), though other studies have showed little influence of power loss on clinically relevant parameters (Kung *et al.*, 2013; Baretta *et al.*, 2011).

There have been a number of important studies illustrating the use of multiscale modeling and surgical planning in pediatric cardiology. Closed-loop models have been used

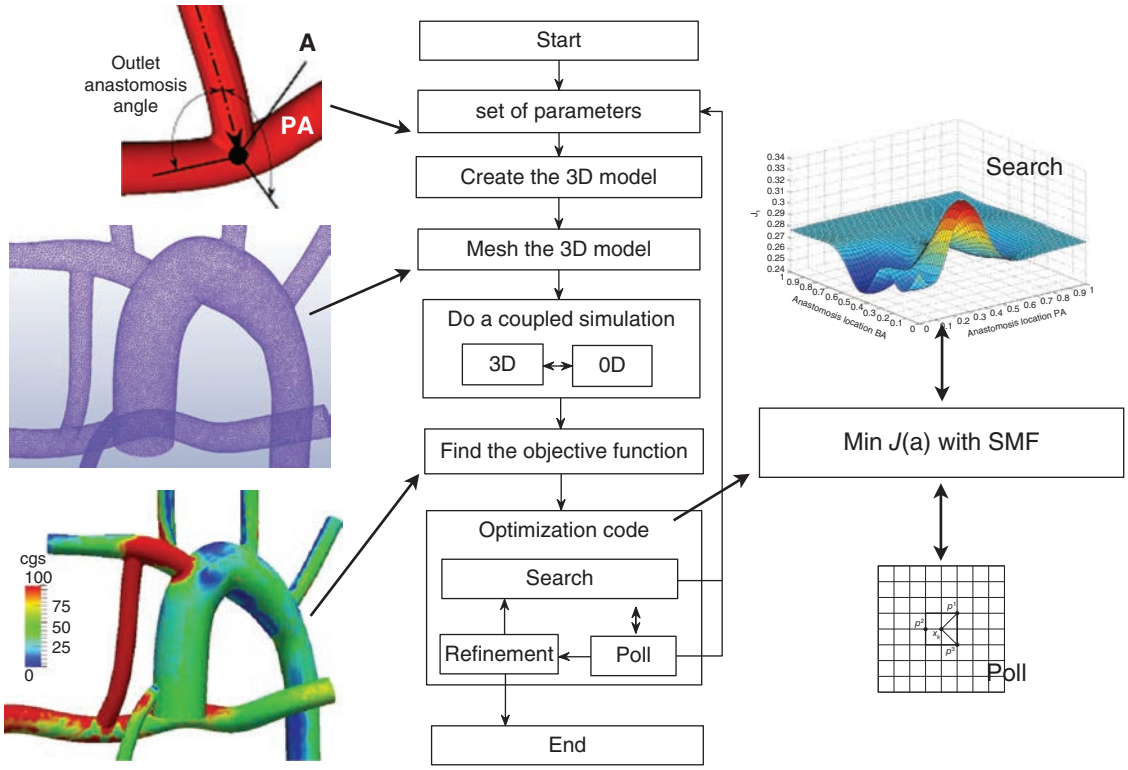

Figure 8. Steps required for automated shape optimization using the surrogate management framework in an idealized model of the Blalock–Taussig shunt surgery to treat single ventricle patients: (1) geometry parameterization, (2) meshing, (3) flow simulation, and (4) optimization algorithm to produce new design parameter set.

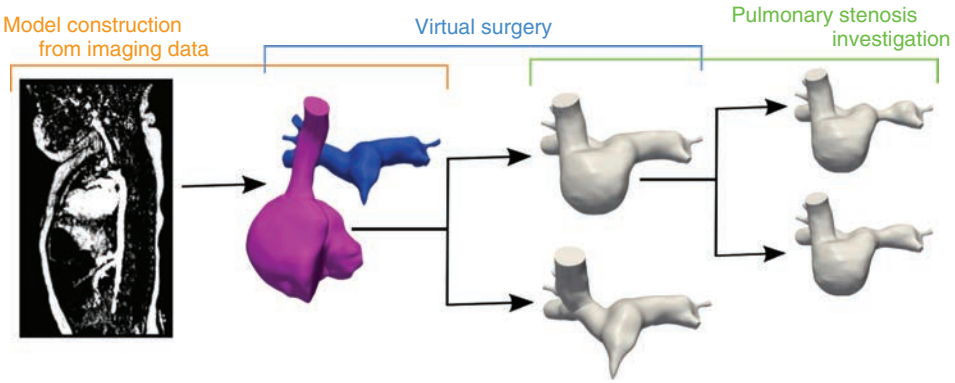

Figure 9. Modeling process for virtual surgery, beginning with model construction from imaging data followed by virtual surgery (a) and the patient-specific stage one models for two patients (b). The example shown compares the hemi-Fontan and Glenn surgeries in single ventricle palliation, as well as surgical correction of pulmonary stenosis.

to devise a protocol for simulating exercise physiology (Kung *et al.*, 2014) and to compare surgical versus hybrid approaches for stage-one single ventricle palliation (Corsini *et al.*, 2011; Hsia *et al.*, 2011). Mock circuits, with hydraulic elements and following the same principles in the in vitro setting, have also been devised to validate simulations and test surgeries and devices (Vukicevic *et al.*, 2013).

Multiscale modeling is applied to compare competing surgical approaches (Glenn vs hemi-Fontan) for the second-stage surgery in single ventricle repair in Figure 9 (Kung *et al.*, 2013). Multiple surgical options can then be compared in a well-controlled "virtual experiment" since parameter values remain fixed when comparing different surgical geometries and stenosis levels. A key point here

is that since one prescribes circuit element values rather than directly prescribing flow and pressure, the closed-loop model allows for dynamic adjustment of flow and pressure waveforms resulting from changes in geometry without the need to assume static BCs.

5.2 Coronary artery disease

Coronary physiology is challenging to model because coronary flow is out of phase with aortic flow due to ventricular contraction (Hoffman and Spann, 1990). Conventional BCs such as resistance or Windkessel (RCR) models do not capture physiologic coronary waveforms, and many studies have been forced to rely on assumed pressure waveforms or invasively obtained data. The challenge of capturing coronary physiology has been addressed through several different approaches using lumped parameter networks, 1D models, and porosity models. Kim *et al.* introduced specialized coronary lumped parameter BCs in the context of patient-specific modeling (Kim *et al.*, 2010b,c) in which coronary outlet BCs were constructed to account for ventricular contraction through incorporation of the myocardial pressure. An alternate approach is to incorporate the effects of cardiac contraction through a vascular varying elastance model (KRAMS *et al.*, 1989). In this approach, the increased stiffness of the myocardium during systole is postulated to drive the coronary flow by modulating the compliance and resistance of the embedded vessels.

The approach of Kim *et al*. (2010b,c) was extended by Sankaran *et al.* (2012) to model the coronary circulation in a closed loop using the coupling methods reviewed above. This study reproduced the clinically observed diastolic coronary flow peak and the postoperative increases in coronary perfusion, based on noninvasive preoperative clinical data. Bypass graft geometry affected local WSS, wall shear stress gradients (WSSGs), and oscillatory shear index (OSI), and results showed that higher anastomosis angles were more optimal than lower angles, as hypothesised in earlier human *in vivo* studies. Coronary simulations have also been applied recently in the study of aneurysms caused by Kawasaki disease, illustrating the potential of simulations to improve risk stratification for determining appropriate anticoagulation therapy and treatment (Sengupta *et al.*, 2012). Recent work has also uncovered significant differences in hemodynamic and biomechanical parameters between arterial and venous grafts in patient-specific simulations following coronary artery bypass graft (CABG) surgery (Ramachandra *et al.*, 2016). These findings may have important implications for mitigating vein graft failure post CABG surgery. Figure 10 illustrates the use of a closed-loop LPN model of the coronary circulation, with contours of WSS obtained from FSI simulations of a patient following CABG surgery. Noninvasive patient-specific CFD studies of the coronary circulation using MRI were recently performed (Torii *et al.*, 2010), including dynamic motion using an ALE formulation and proximal velocity waveforms acquired by MRI.

Recent studies have introduced a new noninvasive method for FFR predictions using patient-specific simulations (Taylor *et al.*, 2013), with promising comparisons between simulated and clinical data reported in recent clinical trials (Nakazato *et al*., 2012; Koo *et al.*, 2011; Min *et al.*, 2012; Nørgaard *et al.*, 2014; Miyoshi *et al.*, 2015). These methods have been demonstrated to significantly improve the diagnosis of coronary artery disease and have the potential for significant reductions in the cost of care (Douglas *et al.*, 2015; Hlatky *et al.*, 2013).

Comprehensive multiscale models of the coronary circulation have also been provided by Smith and others, primarily using a coupled 1D modeling approach (Smith, 2004). Pulsatile flow in a distributed 1D coronary network is described, in which regional myocardial stresses were applied on the vessels, calculated from an anisotropic finite deformation model of the beating heart (Smith, 2004). Coronary models have recently been extended to model the interaction between coronary perfusion and myocardial mechanics using poroelasticity (Vankan *et al.*, 1997; Cookson *et al.*, 2012). Additional details on coronary multiscale modeling can be found in the excellent review of Lee and Smith (2012).

5.3 Transitional hemodynamic stages

Virtually, all blood flow simulation work to-date has been done under the assumption of fixed, cycle-to-cycle periodic pulsatile conditions. However, in order to provide adequate blood supply to different vascular territories and to keep blood pressure relatively constant under a wide range of different physiological conditions, such as changes in posture, digestion, stress, trauma, or exercise, the circulatory system is equipped with several regulatory feedback and feedforward mechanisms. Affecting local and global properties such as individual vessel tone and heart rate, these feedback mechanisms enable the regulation of pressure and flow throughout the body. Therefore, in order to model changes in physiologic states, we must develop control system workflows in the multiscale simulation framework, in which error signals, response functions, and communication between different components of the system (typically represented via reduced-order models) are enabled.

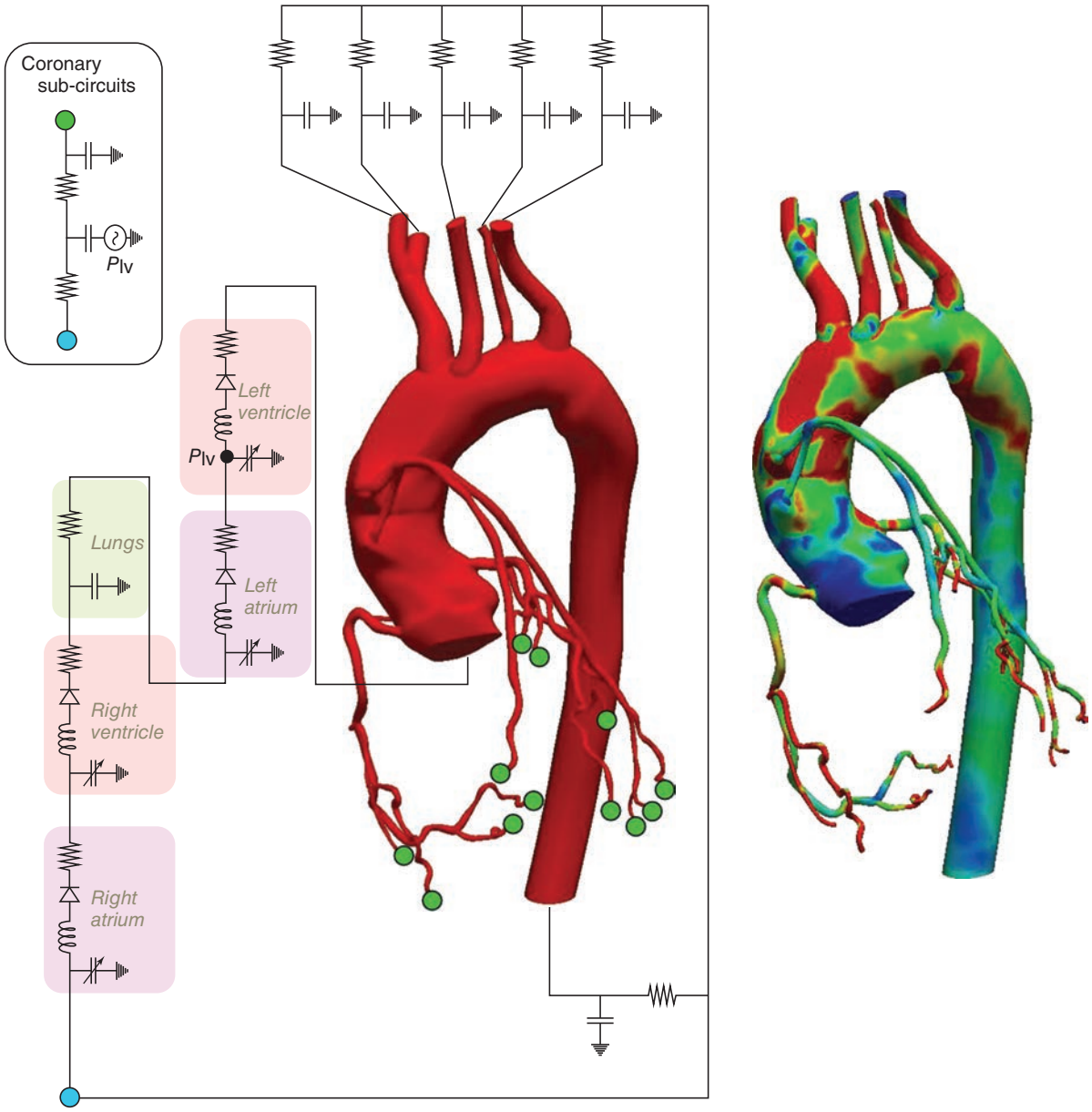

Figure 10. Example of a closed-loop lumped parameter network coupled to a patient-specific model of coronary artery bypass graft surgery (upper) and a simulated wall shear stress field (lower) (contours WSS magnitude min 0, max 15 dynes cm^{-2}).

5.3.1 Models of global control – the baroreflex

One key regulatory mechanism is the arterial baroreflex – a negative feedback system that responds to short-term variations in pressure by altering the state of the systemic circulation in order to maintain pressure homeostasis. The baroreflex can be broadly divided into three components: (i) the baroreceptors cells, (ii) the vasomotor control center, and (iii) the sympathetic and parasympathetic nervous systems (Figure 11).

Connected to the vasomotor center of the brain via the afferent pathways, the baroreceptor cells modulate their nervous firing rate when the magnitude of stretch deviates from prior baseline values. Equipped with a memory of 1–2 days, these cells are specialized for the role of short-term pressure regulation (Guyton, 1992). The vasomotor center of the brain interprets the afferent nervous activity of the baroreceptors. Altered afferent activity arising from variations in pressure generates efferent activity within the vasomotor center that is transmitted to different anatomical

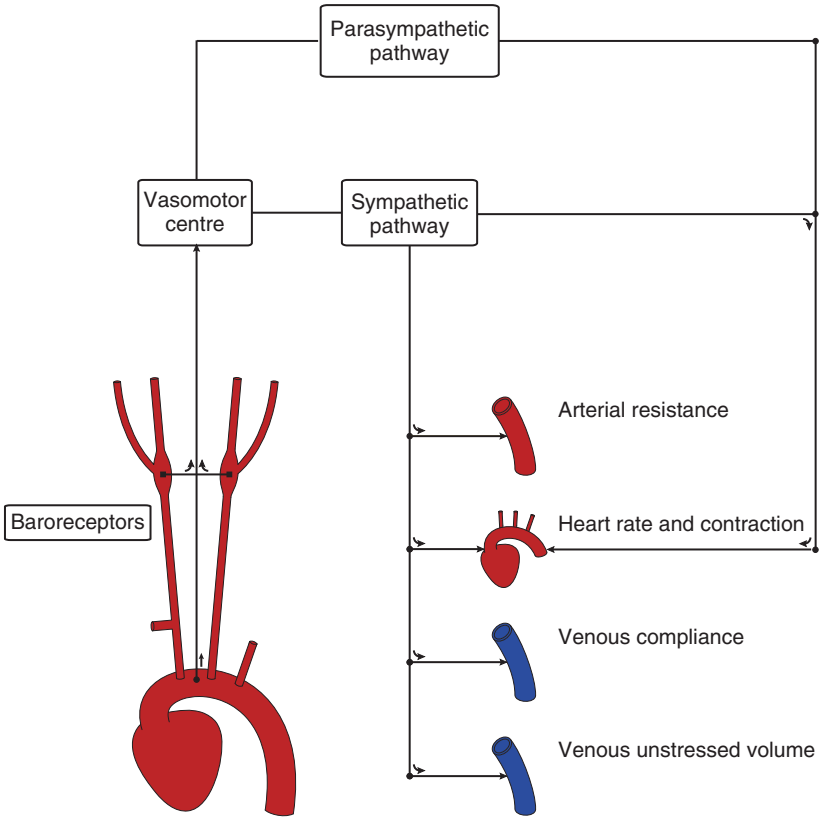

Figure 11. Schematic of the main components of the baroreflex. Here, the filled square and filled circle symbols refer to the location of the carotid and aortic baroreceptors, respectively (Lau and Figueroa, 2015). (Lau, https://link.springer.com/article/10.1007%2Fs10237-014-0645-x. Used under CC BY 4.0 https://creativecommons.org/licenses/by/4.0/.)

regions of the systemic circulation. This efferent activity travels through two different pathways, known as the sympathetic response and the parasympathetic response, which aim to restore blood pressure to baseline values. The sympathetic and parasympathetic nervous systems innervate the heart and the peripheral vessels, thereby allowing control of heart rate, cardiac contractility, and vessel vasoconstriction. Increased sympathetic activity results in vasoconstriction of the peripheral vessels, increased heart rate, and increased cardiac contractility factors that all have a restorative effect on blood pressure. Conversely, increased parasympathetic activity decreases heart rate and cardiac contractility, thereby reducing systemic blood pressure (Guyton, 1992). Changes in sympathetic and parasympathetic activities occur simultaneously, for example, an increase in sympathetic activity and a decrease in parasympathetic activity are effected when an increase in blood pressure is desired. Via the coordinated response of these activities, the baroreflex rapidly alters the hemodynamics throughout the systemic circulation, exerting global control of the pressure on a beat-by-beat basis. The ability to transiently alter pressure is clinically measured using an index referred to as the baroreflex sensitivity (La Rovere *et al.*, 2008). Defined as the change in peak systolic pressure over successive beats, this sensitivity is a direct measure of the strength of the baroreflex response and has been shown to be an indicator of mortality in diseased states (La Rovere *et al.*, 2001). Several mathematical models of the baroreflex have been proposed thus far, with each examining different aspects of this coupled system. So far, these approaches have been mostly implemented using 0D (e.g., lumped parameter network) models. Early 0D baroreflex models include those developed by Ottesen (1997) and (Ursino *et al.* (1998); these two models explored the long-term stability of the negative feedback mechanism and the effectiveness of the baroreflex in cases of blood loss (trauma), respectively. Other 0D models have examined the baroreflex under controlled scenarios, such as the tilt test in Heldt *et al.* (2002), where orientation-dependent pressures were imposed in different anatomical regions. More recently, (Beard *et al.* (2013) examined the role of the baroreflex in combination with other regulatory pressure mechanisms,

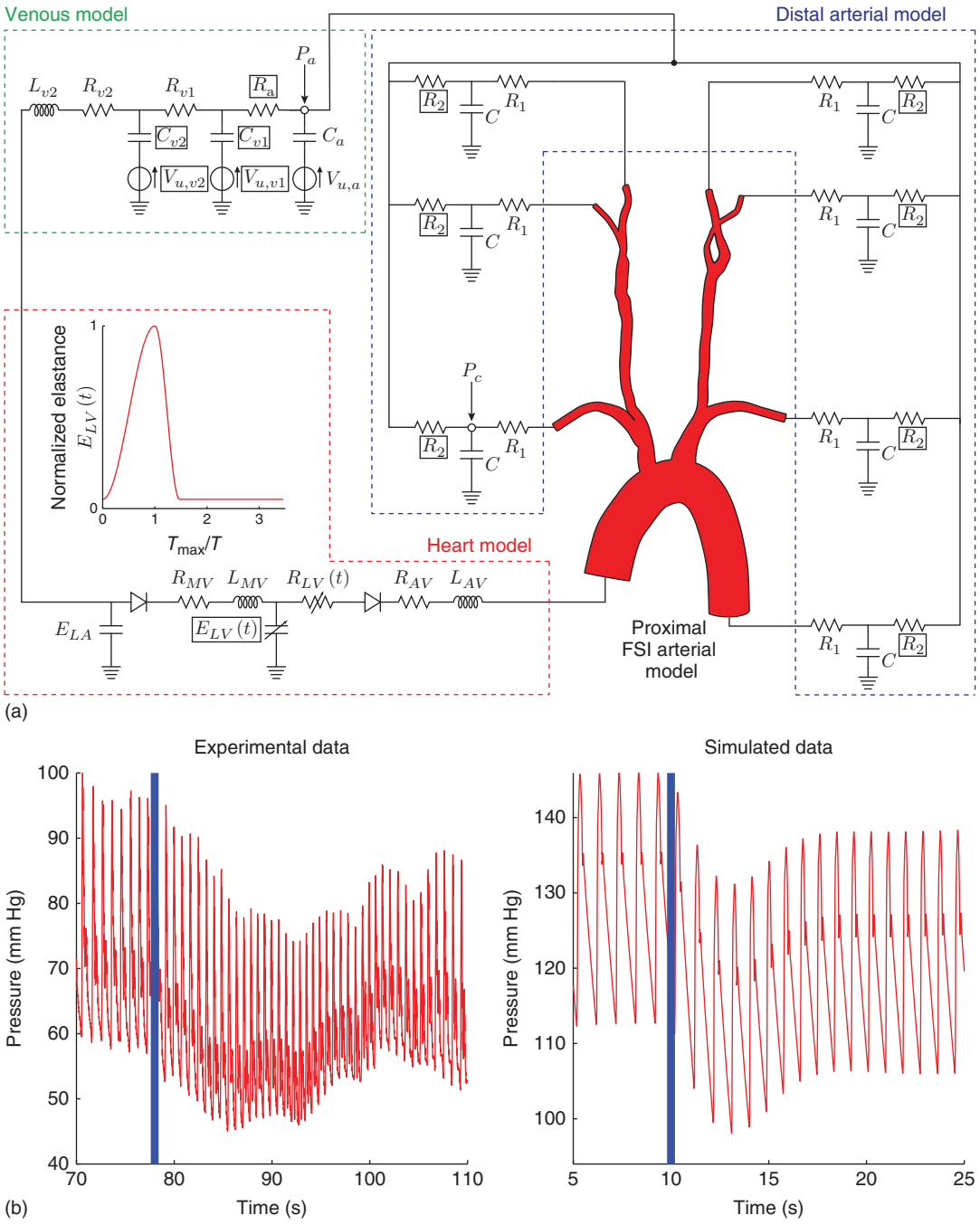

Figure 12. (a) Model of the systemic circulation with both 3D and 0D components. Here, the boxed variables (left ventricular elastance E_{LV}, distal resistances R_{2i}, arteriole resistance R_a, venous compliances C_{vi}, and unstressed volumes Vu, vi) denote controlled quantities. (b) Comparison of experimental and simulated pressure recovery during the head up tilt test. The simulated data is taken from the left internal carotid vessel in the model depicted in (a). In both plots, the start of the tilt test is denoted with the solid blue line. Data and simulation show a close qualitative agreement in the pressure traces before, during, and after the tilt test.

such as the renin–angiotensin system, to explore the effects of chronic baroreflex stimulation. Notable 3D–0D models of the baroreflex include those developed by Kim *et al*. (2010a) and Lau and Figueroa (2015). Kim employed a closed-loop model of the circulation where a baroreflex response based on the model reported by Ottesen *et al.* (2004) was triggered by imposing arbitrary changes in the peripheral resistance of the systemic circulation. Lau and Figueroa developed

a more realistic baroreflex trigger, given by a change in posture of the individual, such as those experienced during a tilt test. That approach enabled the explicit control (rather than direct imposition) of the peripheral systemic resistance, one of the key factors effected by the baroreflex system. Results obtained with this model are depicted in Figure 12.

5.3.2 Models of local control

In the human circulation, in addition to the global control mechanism of the baroreflex, there are localized feedback and feedforward mechanisms in certain vascular beds that operate jointly with the baroreflex to regulate pressure and flow in areas such as the cerebral, coronary, and renal circulations. Local changes in pressure, WSS, and/or metabolite concentrations trigger vascular smooth muscle activation, affecting the arteriolar resistance through changes in vessel diameter. Most of the key contributions in the simulation of local auto-regulations have been developed in the context of 0D models. Ursino developed models for cerebral control (Ursino, 1988; Ursino and Lodi, 1997; Ursino *et al.*, 1998), Layton has recently used mathematical models of renal auto-regulation (Sgouralis and Layton, 2014), Feigl has developed models of coronary auto-regulation involving both feedback and feedforward components (Miyashiro and Feigl, 1993; Tune *et al.*, 2002). Pries and Secomb developed models for structural (longer-term) adaptation in the microcirculation (Pries *et al.*, 2001). Recently, Arthurs *et al.* (2016) developed a 3D–0D model of coronary autoregulation, including both feedback and feedforward mechanisms and used clinical data on coronary flow and pressure during moderate exercise. The model could reproduce changes in coronary hemodynamics over a time interval of 20 min by just imposing the patient's heart rate and peak pressure as inputs (Figure 13).

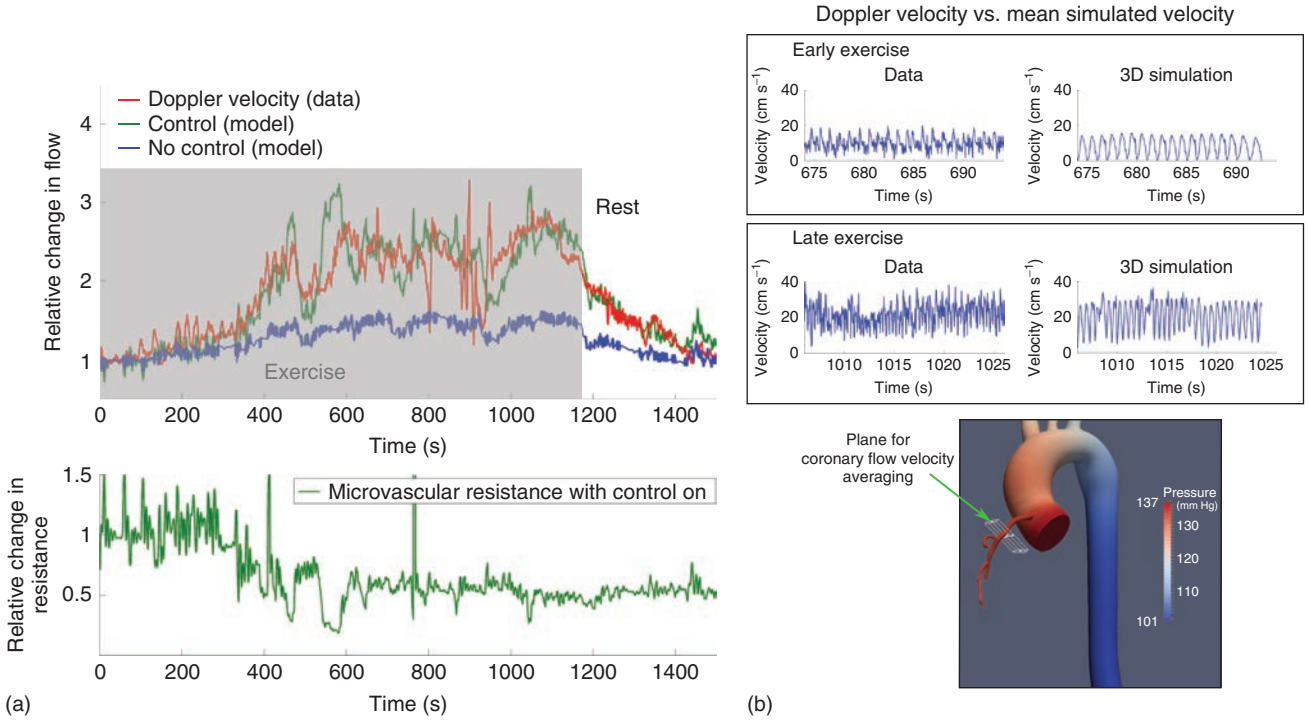

Figure 13. (a) Simulation of auto-regulation in coronary flow using patient data and a 3D–0D model featuring feedback and feedforward control mechanisms (Arthurs *et al.*, 2016). Good agreement is observed between the proportional change in coronary volumetric flow in the control model (green line) and the patient-recorded coronary flow velocity data (red line). Without control of the coronary microvascular resistance, it is not possible to reproduce the patient coronary flow response (blue line). The microvascular resistance is approximately halved during exercise by the control system when it is active. (Arthurs, http://ajpheart.physiology.org/content/310/9/H1242. Used under CC BY 3.0 https://creativecommons.org/licenses/by/3.0/.) (b) Direct comparison between simulated and patient-recorded coronary flow velocity in the proximal region of the coronary tree, under near resting flow conditions (early exercise), and at high flow (late exercise). The snapshot of the pressure distribution is at an early point of systole.

6 FUTURE CHALLENGES

6.1 Adoption challenges

Cardiovascular simulations hold value as both a research tool and, ultimately, a clinical tool to test novel surgical concepts and individualize treatments for patients suffering from congenital and acquired heart disease. Simulations can also augment clinical imaging data and physician expertise by providing predictions of patient risk for disease progression or adverse outcomes. However, several roadblocks have prevented wider adoption of simulations for clinical use. Among these are the high cost of simulations, often requiring hours to days in high performance computing facilities, the need for more extensive *in vivo* validation, and the challenges of developing and incorporating models of physiologic and biologic mechanisms.

There is a pressing need to develop standards and provide worflows for code validation and verification. The ever-increasing number of computer codes (commercial and academic) used to perform cardiovascular simulations makes it easier than ever to produce solutions. However, these solutions are often times unphysiological, due to limitations either in the software (e.g., inhability to incorporate meaningful inflow and outflow BCs) or in the operator (e.g., unfamiliarity with key aspects of the computational modeling workflow). Recently, a number of "computer challenges" have been proposed to test computer codes under different controlled scenarios (experimental or image-based) (Stewart *et al.*, 2012; Steinman *et al.*, 2013; Janiga *et al.*, 2015; Berg *et al.*, 2015). These challenges have sometimes revealed an alarming variability in the results reported by the different users (Stewart *et al.*, 2012). The solution to this problem may require the development of an acreditation system to certify that a given user has the required knowledge and expertise to perform meaningful blood flow analyses with properly tested computer codes.

6.2 New application areas

While much of the field has focused on vascular hemodynamics, the field of integrative cardiac modeling provides a rich diversity of problems that have yet to be explored.

Prediction of thrombus formation is both notoriously challenging and crucial to clinical applications involving stroke, plaque rupture and myocardial infarction, deep vein thrombosis, and embolism. The coagulation cascade is a complex biochemistry system that is strongly influenced by mechanical factors and thus neither can be examined independently. Because thrombus formation is highly multiscale, accurate models should incorporate fine-to-coarse-grained information about blood biochemistry that can be coupled with patient-specific hemodynamic models. While several groups have had initial success developing biochemistry models of the coagulation cascade, there remains a need for validation against experiments using whole blood, and against clinical data, and for numerical frameworks that can effectively bridge multiple scales. Only with these developments will such models be successfully translated to the clinical realm for thrombus prevention and risk assessment.

Finally, development of integrative models of cardiac function, including myocardial contraction, electrophysiology, ventricular hemodynamics, and valve motion, will allow the field to move from the vascular to the cardiac realm. Such models will require integration of multiphysics finite element tools with capabilities for large-deformation FSI to capture ventricular contraction and heart valve dynamics, nonlinear and viscoelastic material models, cardiac mechanics models of active heart contraction, and electrophysiology. This will enable new research directions in congenital and acquired cardiac diseases including heart failure, cardiomyopathy, cardiac remodeling, valve dysfunction, aortic dissection, ventricular thrombosis, and cardiac device design.

7 RELATED CHAPTERS

(*See also* **Finite Element Methods**, **Arbitrary Lagrangian–Eulerian Methods**, **Multiscale and Stabilized Methods**, **Incompressible Viscous Flows**, **Variational Multiscale Methods in Computational Fluid Dynamics**)

ACKNOWLEDGEMENTS

CAF gratefully acknowledges the support by the University of Michigan Frankel Cardiovascular Center, the Edward B. Diethrich M.D. professorship, the United States National Institutes of Health Grants 2R01HL105297 and U01HL135842, and the European Research Council under the European Union's Seventh Framework Programme (FP/2007-2013) with grant number 307532.

REFERENCES

Abraham F, Behr M and Heinkenschloss M. Shape optimization in unsteady blood flow: a numerical study of non-newtonian effects. *Comput. Methods Biomech. Biomed. Eng.* 2005; **8**:201–212.

Agoshkov V, Quarteroni A, Rozza G. A mathematical approach in the design of arterial bypass anastomoses using unsteady stokes equations. *J. Sci. Comput.* 2006a; **28**:139–161.

Agoshkov V, Quarteroni A and Rozza G. Shape design in aorto-coronaric bypass anastomoses using perturbation theory. *SIAM J. Numer. Anal.* 2006b; **44**(1):367–384.

Alastruey J, Khir AW, Matthys KS, Segers P, Sherwin SJ, Verdonck PR, Parker KH and Peiró J. Pulse wave propagation in a model human arterial network: assessment of 1-D visco-elastic simulations against in vitro measurements. *J. Biomech.* 2011; **44**(12):2250–2258. doi: 10.1016/j.jbiomech.2011.05.041.

Alastruey J, Parker KH, Peiró J and Sherwin SJ. Lumped parameter outflow models for 1-D blood flow simulations: effect on pulse waves and parameter estimation. *Commun. Comput. Phys.* 2008; **4**:317–336.

Alastruey J, Xiao N, Fok H, Schaeffter T and Figueroa CA On the impact of modelling assumptions in multi-scale, subject-specific models of aortic haemodynamics. *J. R. Soc. Interface* 2016; **13**(119):20160 073. DOI: 10.1098/rsif.2016.0073.

Arthurs CJ, Lau KD, Asrress KN, Redwood SR and Figueroa CA. A mathematical model of coronary blood flow control: simulation of patient-specific three-dimensional hemodynamics during exercise. *Am. J. Physiol. Heart Circ. Physiol.* 2016; **310**(9):H1242–H1258, doi: 10.1152/ajpheart.00 517.2015.

Audet C. Convergence results for pattern search algorithms are tight. *Optim. Eng.* 2004; **5**(2):101–122.

Audet C and Dennis JE Jr. Analysis of generalized pattern searches. *SIAM J. Optim.* 2003; **13**(3):889–903.

Audet C and Dennis JE Jr. A pattern search filter method for nonlinear programming without derivatives. *SIAM J. Optim.* 2004; **14**(4):980–1010.

Audet C and Dennis JE Jr. Mesh adaptive direct search algorithms for constrained optimization. *SIAM J. Optim.* 2006; **17**(1):188–217.

Baaijens FPT. A fictitious domain/mortar element method for fluid-structure interaction. *Int. J. Numer. Methods Fluids* 2001; **35**(7):743–761.

Babuška I, Nobile F and Tempone R. A stochastic collocation method for elliptic partial differential equations with random input data. *SIAM J. Numer. Anal.* 2007; **45**(3):1005–1034.

Baek S, Rajagopal KR and Humphrey JD. A theoretical model of enlarging intracranial fusiform aneurysms. *J. Biomech. Eng.* 2006; **128**(1):142–149.

Bagchi P. Mesoscale simulation of blood flow in small vessels. *Biophys. J.* 2007; **92**(6):1858–1877.

Baretta A, Corsini C, Yang W, Vignon-Clementel I, Marsden A, Feinstein J, Hsia TY, Dubini G, Migliavacca F and Pennati G. Virtual surgeries in patients with congenital heart disease: a multiscale modelling test case. *Philos. Trans. R. Soc. London, Ser. A* 2011; **369**(1954):4316–4330.

Bazilevs Y, Calo V, Zhang Y and Hughes TJ. Isogeometric fluid–structure interaction analysis with applications to arterial blood flow. *Comput. Mech.* 2006; **38**(4-5):310–322.

Beard DA, Pettersen KH, Carlson BE, Omholt SW and Bugenhagen SM. A computational analysis of the long-term regulation of arterial pressure. *F1000Res.* 2013; **2**:208, 2 doi: 10.12688/f1000research.2-208.v2.

Berg P, Roloff C, Beuing O, Voss S, Sugiyama SI, Aristokleous N, Anayiotos AS, Ashton N, Revell A, Bressloff NW, Phase II *et al.* The computational fluid dynamics rupture challenge 2013-variability of hemodynamic simulations in two intracranial aneurysms. *J. Biomech. Eng.* 2015; **137**(12):121 008.

Bessems D, Rutten M and Van De Vosse F. A wave propagation model of blood flow in large vessels using an approximate velocity profile function. *J. Fluid Mech.* 2007; **580**:145–168, doi: 10.1017/S0022112007005344.

Blanco PJ, Watanabe SM, Passos MARF, Lemos PA and Feijoo RA. An anatomically detailed arterial network model for one-dimensional computational hemodynamics. *IEEE Trans. Biomed. Eng.* 2015; **62**(2):736–753.

Booker AJ, Dennis JE Jr., Frank PD, Serafini DB, Torczon V, Trosset MW. A rigorous framework for optimization of expensive functions by surrogates. *Struct. Optim.* 1999; **17**(1):1–13.

Caro CG, Fitz-Gerald JM and Schroter RC. Atheroma and arterial wall shear: observation, correlation and proposal of a shear dependent mass transfer mechanism for atherogenesis. *Proc. R. Soc. London, Ser. B: Biol. Sci.* 1971; **177**:109–159.

Cebral JR, Castro MA, Appanaboyina S, Putman CM, Millan D and Frangi AF. Efficient pipeline for image-based patient-specific analysis of cerebral aneurysm hemodynamics: technique and sensitivity. *IEEE Trans. Med. Imaging* 2005a; **24**(4):457–467.

Cebral JR, Castro MA, Burgess JE, Pergolizzi RS, Sheridan MJ and Putman CM. Characterization of cerebral aneurysms for assessing risk of rupture by using patient-specific computational hemodynamics models. *Am. J. Neuroradiol.* 2005b; **26**(10):2550–2559.

Chapelle D, Fragu M, Mallet V and Moireau P. Fundamental principles of data assimilation underlying the Verdandi library: applications to biophysical model personalization within euHeart. *Med. Biol. Eng. Comput.* 2013; **51**(11):1221–1233.

Choy JS and Kassab GS. Scaling of myocardial mass to flow and morphometry of coronary arteries. *J. Appl. Physiol.* 2008; **104**(5):1281–1286.

Coogan JS, Taylor CA, Humphrey JD and Figueroa CA. Computational simulations of hemodynamic alterations and remodeling of the thoracic aorta, coronary, and cerebral vascular beds following distal aortic coarctation. *Biomech. Model. Mechanobiol.* 2013; **12**(1):79–93. doi: 10.1007/s10237-012-0383-x

Cookson A, Lee J, Michler C, Chabiniok R, Hyde E, Nordsletten D, Sinclair M, Siebes M and Smith N. A novel porous mechanical framework for modelling the interaction between coronary perfusion and myocardial mechanics. *J. Biomech.* 2012; **45**(5):850–855.

Corsini C, Cosentino D, Pennati G, Dubini G, Hsia T and Migliavacca F. Multiscale models of the hybrid palliation for hypoplastic left heart syndrome. *J. Biomech.* 2011; **44**(4):767–770.

Cuomo F, Ferruzzi J, Humphrey JD and Figueroa CA. An experimental-computational study of catheter induced alterations in pulse wave velocity in anesthetized mice. *Ann. Biomed. Eng.* 2015; **43**(7):1555–1570, doi: 10.1007/s10439-015-1272-0.

Davis C. Theory of positive linear dependence. *Am. J. Math.* 1954; **76**(4):448–474.

DeGroff CG. Modeling the fontan circulation: where we are and where we need to go. *Pediatr. Cardiol.* 2008; **29**:3–12.

De Hart J, Peters GWM, Schreurs PJG and Baaijens FPT. A three-dimensional computational analysis of fluid-structure interaction in the aortic valve. *J. Biomech.* 2003; **36**(1):103–112.

De Hart J, Peters GWM, Schreurs PJG and Baaijens FPT. Collagen fibers reduce stresses and stabilize motion of aortic valve leaflets during systole. *J. Biomech.* 2004; **37**(3):303–311.

de Leval MR, Dubini G *et al.* Use of computational fluid dynamics in the design of surgical procedures: application to the study of competitive flows in cavopulmonary connections. *J. Thorac. Cardiovasc. Surg.* 1996; **111**(3):502–513.

Dillon-Murphy D, Noorani A, Nordsletten D and Figueroa CA. Multi-modality image-based computational analysis of haemodynamics in aortic dissection. *Biomech. Model. Mechanobiol.* 2016; **15**(4):857–876. doi: 10.1007/s10237-015-0729-2

Douglas P, Pontone G, Hlatky M, Patel M, Norgaard B, Byrne R, Curzen N, Purcell I, Gutberlet M, Rioufol G *et al.* Clinical outcomes of fractional flow reserve by computed tomographic angiography-guided diagnostic strategies vs. usual care in patients with suspected coronary artery disease: the prospective longitudinal trial of ffrct: outcome and resource impacts study. *Eur. Heart J.* 2015; **36**(47):3359–3367.

Dubini G, de Leval MR, Pietrabissa R, Montevecchi FM and Fumero R. A numerical fluid mechanical study of repaired congenital heart defects: application to the total cavopulmonary connection. *J. Biomech.* 1996; **29**(1):111–121.

Ensley AE, Lynch P, Chatzimavroudis GP, Lucas C, Sharma S and Yoganathan AP. Toward designing the optimal total cavopulmonary connection: an in vitro study. *Ann. Thorac. Surg.* 2000a; **68**:1384–1390.

Ensley AE, Ramuzat A, Healy TM, Chatzimavroudis GP, Lucas C, Sharma S, Pettigrew R and Yoganathan AP. Fluid mechanic assessment of the total cavopulmonary connection using magnetic resonance phase velocity mappaing and digital particle image velocimetry. *Ann. Biomed. Eng.* 2000b; **28**:1172–1183.

Esmaily-Moghadam M, Bazilevs Y, Hsia TY, Vignon-Clementel I and Marsden A. A comparison of outlet boundary treatments for prevention of backflow divergence with relevance to blood flow simulations. *Comput. Mech.* 2011; **48**:277–291.

Esmaily-Moghadam M, Bazilevs Y and Marsden AL. A new preconditioning technique for implicitly coupled multidomain simulations with applications to hemodynamics. *Comput. Mech.* 2013a; **52**(5):1141–1152, doi: 10.1007/s00466-013-0868-1.

Esmaily-Moghadam M, Vignon-Clementel I, Figliola R and Marsden A. A modular numerical method for implicit 0D/3D coupling in cardiovascular finite element simulations. *J. Comput. Phys.* 2013b; **244**(1):63–79.

Esmaily-Moghadam M, Migliavacca F, Vignon-Clementel IE, Hsia TY and Marsden AL. Modeling of congenital hearts alliance (MOCHA) investigators. Optimization of shunt placement for the norwood surgery using multi-domain modeling. *J. Biomech. Eng.* 2012; **134**(5):051 002.

Figueroa CA, Baek S, Taylor CA and Humphrey JD. A computational framework for fluid–solid–growth modeling in cardiovascular simulations. *Comput. Meth. Appl. Mech. Eng.* 2009; **198**(45-46):3583–3602, doi: 10.1016/j.cma.2008.09.013.

Figueroa CA, Vignon-Clementel IE, Jansen KE, Hughes TJ and Taylor CA. A coupled momentum method for modeling blood flow in three-dimensional deformable arteries. *Comput. Methods Appl. Mech. Eng.* 2006; **195**(41-43):5685–5706. doi: 10.1016/j.cma.2005.11.011

Fontan F and Baudet E. Surgical repair of tricuspid atresia. *Thorax* 1971; **26**:240–248.

Formaggia L, Lamponi D and Quarteroni A. One-dimensional models for blood flow in arteries. *J. Eng. Math.* 2003; **47**(3-4):251–276.

Friedman M, Hutchins GM, Bargeron CB, Daters O and Mark FF. Correlation between intimal thickness and fluid shear in human arteries. *Atherosclerosis* 1981; **39**:425–436.

Fung Y. *Biodynamics Circulation*. Springer-Verlag: New York, 1984.

Galt SW, Zwolak R, Wagner R and Gilbertson J. Differential response of arteries and vein grafts to blood flow reduction. *J. Vasc. Surg.* 1993; **17**:563–570.

Gerbeau JF and Vidrascu M. A quasi-Newton algorithm based on a reduced model for fluid-structure interaction problems in blood flows. *ESAIM-Math. Modell. Num.* 2003; **37**(4):631–647, doi: 10.1051/m2an:2003049.

Gerbeau JF, Vidrascu M and Frey P. Fluid-structure interaction in blood flows on geometries coming from medical imaging. *Comput. Struct.* 2005; **83**(2-3):155–165.

Ghanem R and Kruger R. Numerical solution of spectral stochastic finite element systems. *Comput. Methods Appl. Mech. Eng.* 1996; **129**(3):289–303.

Ghanem RG and Spanos PD. *Stochastic Finite Elements: A Spectral Approach*. Springer-Verlag: New York, 1991.

Glowinski R, Pan TW and Periaux J. A Lagrange multiplier/fictitious domain method for the numerical simulation of incompressible viscous flow around moving rigid bodies: (I) case where the rigid body motions are known a priori. *C.R. Acad. Sci. Ser. I - Math.* 1997; **324**(3):361–369, doi: 10.1016/S0764-4442(99)80376-0.

Griffith BE, Luo X, McQueen DM and Peskin CS. Simulating the fluid dynamics of natural and prosthetic heart valves using the immersed boundary method. *Int. J. Appl. Mech.* 2009; **01**(01):137–177.

Gundert TJ, Marsden AL, Yang W and LaDisa JF. Optimization of cardiovascular stent design using computational fluid dynamics. *Trans. ASME J. Biomech. Eng.* 2012a; **134**(1):011002.

Gundert TJ, Marsden AL, Yang W, Marks DS and LaDisa JF. Identification of hemodynamically optimal coronary stent designs based on vessel caliber. *IEEE Trans. Biomed. Eng. Biomed. Eng.* 2012b; **59**(7):1992–2002.

Guyton A. *Human Physiology and Mechanisms of Disease*. W.B. Saunders, 1992.

Healy TM, Lucas C and Yoganathan AP. Noninvasive fluid dynamic power loss assessments for total cavopulmonary connections using the viscous dissipation function: a feasibility study. *J. Biomech. Eng.* 2001; **123**:317–324.

Heldt T, Shim EB, Kamm RD and Mark RG. Computational modeling of cardiovascular response to orthostatic stress. *J. Appl. Physiol.* 2002; **92**(3):1239–1254, doi: 10.1152/japplphysiol.00241.2001.

Hlatky MA, Saxena A, Koo BK, Erglis A, Zarins CK and Min JK. Projected costs and consequences of computed tomography-determined fractional flow reserve. *Clin. Cardiol.* 2013; **36**(12):743–748, doi: 10.1002/clc.22205.

Hoffman J and Spann JE. Pressure-flow relations in coronary circulation. *Physiol. Rev.* 1990; **70**(2):331–390.

Holenstein R, Niederer P and Anliker M. A viscoelastic model for use in predicting arterial pulse waves. *J. Biomech. Eng.* 1980; **102**(4):318–325.

Holzapfel Ga, Gasser TC and Ogden RW. A new constitutive framework for arterial wall mechanics and a comparative study of material models. *J. Elast.* 2000; **61**(1-3):1–48, doi: 10.1023/A:1010835316564.

Hsia TY, Cosentino D, Corsini C, Pennati G, Dubini G and Migliavacca F. Use of mathematical modeling to compare and predict hemodynamic effects between hybrid and surgical norwood palliations for hypoplastic left heart syndrome. *Circulation* 2011; **124**:S204–S210.

Hughes T and Lubliner J. On the 1 dimensional theory of blood flow in the larger vessels. *Math. Biosci.* 1973; **18**:161–170.

Hughes TJR, Liu WK and Zimmermann TK. Lagrangian-Eulerian finite element formulation for incompressible viscous flows. *Comput. Methods Appl. Mech. Eng.* 1981; **29**(3):329–349.

Humphrey J. Vascular adaptation and mechanical homeostasis at tissue, cellular, and sub-cellular levels. *Cell Biochem. Biophys.* 2008; **50**(2):53–78.

Humphrey J and Rajagopal K. A constrained mixture model for growth and remodeling of soft tissues. *Math. Models Methods Appl. Sci.* 2002; **12**(3):407–430, doi: 10.1142/S0218202502001714.

Ismail M, Gravemeier V, Comerford A and Wall W. A stable approach for coupling multidimensional cardiovascular and pulmonary networks based on a novel pressure-flow rate or pressure-only neumann boundary condition formulation. *Int. J. Numer. Methods Biomed. Eng.* 2013; **30**(4):447–469.

Janiga G, Berg P, Sugiyama S, Kono K and Steinman DA. The computational fluid dynamics rupture challenge 2013 – Phase I: prediction of rupture status in intracranial aneurysms. *Am. J. Neuroradiol.* 2015; **36**(3):530–536.

Julier SJ, Uhlmann JK and Durrant-Whyte H. A new method for the nonlinear transformation of means and covariances in filters and estimators. *IEEE Trans. Autom. Control* 2000; **45**(3):477–482.

Kamiya A and Togawa T. Adaptive regulation of wall shear stress to flow change in the canine carotid artery. *Am. J. Physiol.* 1980; **239**:H14–H21.

Kardong K. *Vertebrates: Comparative Anatomy, Function, Evolution*. McGraw-Hill, 2002.

Kassab GS and Fung YC. The pattern of coronary arteriolar bifurcations and the uniform shear hypothesis. *Ann. Biomed. Eng.* 1995; **23**:13–20.

Kay I. *Introduction to Animal Physiology*. Springer-Verlag, 1998.

Kim HJ, Jansen KE and Taylor CA. Incorporating autoregulatory mechanisms of the cardiovascular system in three-dimensional finite element models of arterial blood flow. *Ann. Biomed. Eng.* 2010a; **38**(7):2314–2330, doi: 10.1007/s10439-010-9992-7.

Kim H, Vignon-Clementel I, Coogan J, Figueroa CA, Jansen K and Taylor C. Patient-specific modeling of blood flow and pressure in human coronary arteries. *Ann. Biomed. Eng.* 2010b; **38**(10):3195–3209. doi: 10.1007/s10439-010-0083-6

Kim H, Vignon-Clementel I, Figueroa CA, Jansen K and Taylor C. Developing computational methods for three-dimensional finite element simulations of coronary blood flow. *Finite Elem. Anal. Des.* 2010c; **46**(6):514–525. doi: 10.1016/j.finel.2010.01.007

Kim HJ, Vignon-Clementel IE, Figueroa CA, LaDisa JF, Jansen KE, Feinstein JA and Taylor CA. On coupling a lumped parameter heart model and a three-dimensional finite element aorta model. *Ann. Biomed. Eng.* 2009; **37**(11):2153–2169. doi: 10.1007/s10439-009-9760-8

Koo BK, Erglis A, Doh JH, Daniels DV, Jegere S, Kim H-S, Dunning A, DeFrance T, Lansky A, Leipsic J, Min JK. Diagnosis of Ischemia-causing coronary stenoses by noninvasive fractional flow reserve computed from coronary computed tomographic angiograms. *J. Am. Coll. Cardiol.* 2011; **58**(19):1989–1997.

Krams R, Sipkema P and Westerhof N. Varying elastance concept may explain coronary systolic flow impediment. *Am. J. Physiol.* 1989; **257**:H1471–H1479.

Kuhl E and Holzapfel GA. A continuum model for remodeling in living structures. *J. Mater. Sci.* 2007; **42**(21):8811–8823.

Kung E, Baretta A, Baker C, Arbia G, Biglino G, Corsini C, Schievano S, Vignon-Clementel I, Dubini G, Pennati G *et al.* Predictive modeling of the virtual hemi-fontan operation for second stage single ventricle palliation: two patient-specific cases. *J. Biomech.* 2013; **46**(2):423–429.

Kung EO, Pennati G, Migliavacca F, Hsia TY, Figliola R, Marsden A and Giardini A. A simulation protocol for exercise physiology in fontan patients using a closed-loop lumped-parameter model. *Trans. ASME J. Biomech. Eng.* 2014; **136**(8):081 007–114.

Kuprat A, Kabilan S, Carson J, Corley R and Einstein D. A bidirectional coupling procedure applied to multiscale respiratory modeling. *J. Comput. Phys.* 2013; **244**:148–167.

La Rovere MT, Pinna G and Raczak G. Baroreflex sensitivity: measurement and clinical implications. *Ann. Noninvasive Electrocardiol.* 2008; **13**(2):191–207.

La Rovere MT, Pinna GD, Hohnloser SH, Marcus FI, Mortara A, Nohara R, Bigger J Jr, Camm AJ, Schwartz PJ, ATRAMIIAT *et al.* Baroreflex sensitivity and heart rate variability in the identification of patients at risk for life-threatening arrhythmias: implications for clinical trials. *Circulation* 2001; **103**(16):2072–2077.

LaDisa JF, Dholakia RJ, Figueroa CA, Vignon-Clementel IE, Chan FP, Samyn MM, Cava JR, Taylor CA and Feinstein JA. Computational simulations demonstrate altered wall shear stress in aortic coarctation patients treated by resection with end-to-end anastomosis. *Congenit. Heart Dis.* 2011a; **6**(5):432–443, doi: 10.1111/j.1747-0803.2011.00553.x.

LaDisa JF, Figueroa CA, Vignon-Clementel IE, Kim HJ, Xiao N, Ellwein LM, Chan FP, Feinstein JA and Taylor CA. Computational simulations for aortic coarctation: representative results from a sampling of patients. *J. Biomech. Eng.* 2011b; **133**(9):091 008–, doi: 10.1115/1.4004996.

Lagana K, Dubini G, Migliavacca F, Pietrabissa R, Pennati G, Veneziani A and Quarteroni A. Multiscale modelling as a tool to prescribe realistic boundary conditions for the study of surgical procedures. *Biorheology* 2002; **39**:359–364.

Lau KD and Figueroa CA. Simulation of short-term pressure regulation during the tilt test in a coupled 3D–0D closed-loop model of the circulation. *Biomech. Model. Mechanobiol.* 2015; **14**(4):915–929.

Le Tallec P and Mouro J. Fluid structure interaction with large structural displacements. *Comput. Methods Appl. Mech. Eng.* 2001; **190**(24-25):3039–3067.

Lee J and Smith NP. The multi-scale modeling of coronary blood flow. *Ann. Biomed. Eng.* 2012; **40**(11):2399–2413.

Lemmon JD and Yoganathan AP. Computational modeling of left heart diastolic function: examination of ventricular dysfunction. *J. Biomech. Eng.* 2000; **122**(4):297–303.

Les A, Shadden S, Figueroa CA, Park J, Tedesco M, Herfkens R, Dalman R and Taylor C. Quantification of hemodynamics

in abdominal aortic aneurysms during rest and exercise using magnetic resonance imaging and computational fluid dynamics. *Ann. Biomed. Eng.* 2010; **38**(4):1288–1313. doi: 10.1007/s10439-010-9949-x

Lewis RM and Torczon V. Rank ordering and positive bases in pattern search algorithms. Technical Report 96–71, Institute for Computer Applications in Science and Engineering, Mail Stop 132C, NASA Langley Research Center, Hampton, VA 23681–2199, 1996.

Lewis RM and Torczon V. A globally convergent augmented Lagrangian pattern search algorithm for optimization with general constraints and simple bounds. *SIAM J. Optim.* 2002; **12**:1075–1089.

Lewis RM and Torczon V. Pattern search algorithms for bound constrained minimization. *SIAM J. Optim.* 1999; **9**:1082–1099.

Lewis RM and Torczon V. Pattern search methods for linearly constrained minimization. *SIAM J. Optim.* 2000; **10**:917–941.

Liu S and Fung Y. Relationship between hypertension, hypertrophy, and opening angle of zero-stress state of arteries following aortic constriction. *J. Biomech. Eng.* 1989; **111**:325–335.

Long C, Marsden A and Bazilevs Y. Fluid–structure interaction simulation of pulsatile ventricular assist devices. *Comput. Mech.* 2013; **52**(5):971–981.

Lophaven SN, Nielsen HB and Søndergaard J. DACE: A MATLAB Kriging toolbox version 2.0. Technical Report IMM-TR-2002-12. Technical University of Denmark: Copenhagen, 2002.

Marchesseau S, Delingette H, Sermesant M, Cabrera-Lozoya R, Tobon-Gomez C, Moireau P, Figueras i Ventura RM, Lekadir K, Hernandez A, Garreau M *et al.* Personalization of a cardiac electromechanical model using reduced order unscented Kalman filtering from regional volumes. *Med. Image Anal.* 2013; **17**(7):816–829.

Markl M, Harloff A, Bley TA, Zaitsev M, Jung B, Weigang E, Langer M, Hennig J and Frydrychowicz A. Time-resolved 3D MR velocity mapping at 3T: improved navigator-gated assessment of vascular anatomy and blood flow. *J. Magn. Reson. Imaging* 2007; **25**(4):824–831.

Marsden AL, Bernstein AJ, Reddy VM, Shadden S, Spilker RL, Chan FP, Taylor CA and Feinstein JA. Evaluation of a novel Y-shaped extracardiac Fontan baffle using computational fluid dynamics. *J. Thorac. Cardiovasc. Surg.* 2009; **137**:394–403.

Marsden A and Esmaily-Moghadam M. Multiscale modeling of cardiovascular flows for clinical decision support. *Appl. Mech. Rev.* 2015; **67**:030 804-1-11.

Marsden AL, Vignon-Clementel IE, Chan F, Feinstein JA and Taylor CA. Effects of exercise and respiration on hemodynamic efficiency in CFD simulations of the total cavopulmonary connection. *Ann. Biomed. Eng.* 2007; **35**(2):250–263.

Matthys KS, Alastruey J, Peiró J, Khir AW, Segers P, Verdonck PR, Parker KH and Sherwin SJ. Pulse wave propagation in a model human arterial network: assessment of 1-D numerical simulations against in vitro measurements. *J. Biomech.* 2007; **40**(15):3476–3486.

Merkow J, Tu Z, Kriegman D and Marsden A. *Structural edge detection for cardiovascular modeling*. Medical Image Computing and Computer-Assisted Intervention – MICCAI 2015: 18th International Conference, Munich, Germany, October 5-9, 2015, Proceedings, Part III, 2015; 735–742, doi: 10.1007/978-3-319-24574-4_88.

Migliavacca F, Dubini G, Bove EL and de Leval MR. Computational fluid dynamics simulations in realistic 3-D geometries of the total cavopulmonary anastomosis: the influence of the inferior caval anastomosis. *J. Biomech. Eng.* 2003; **125**:805–813.

Min JK, Leipsic J, Pencina MJ, Berman DS, Koo BK, van Mieghem C, Erglis A, Lin FY, Dunning AM, Apruzzese P *et al.* Diagnostic accuracy of fractional flow reserve from anatomic CT angiography. *JAMA* 2012; **308**(12):1237–1245, doi: 10.1001/2012.jama.11274.

Miyashiro J and Feigl E. Feedforward control of coronary blood flow via coronary β-receptor stimulation. *Circ. Res.* 1993; **73**(2):252–263.

Miyoshi T, Osawa K, Ito H, Kanazawa S, Kimura T, Shiomi H, Kuribayashi S, Jinzaki M, Kawamura A, Bezerra H *et al.* Non-invasive computed fractional flow reserve from computed tomography (CT) for diagnosing coronary artery disease. *Circ. J.* 2015; **79**(2):406–412, doi: 10.1253/circj.CJ-14-1051.

Moireau P, Bertoglio C, Xiao N, Figueroa CA, Taylor CA, Chapelle D and Gerbeau JF. Sequential identification of boundary support parameters in a fluid-structure vascular model using patient image data. *Biomech. Model. Mechanobiol.* 2012; **12**(3):475–496. doi: 10.1007/s10237-012-0418-3

Moore JE Jr and Ku DN. Pulsatile velocity measurements in a model of the human abdominal aorta under resting conditions. *J. Biomech. Eng.* 1994; **116**:337–346.

Moore JE Jr, Xu C, Glagov S, Zarins CK and Ku DN. Fluid wall shear stress measurements in a model of the human abdominal aorta: oscillatory behavior and relationship to atherosclerosis. *Atherosclerosis* 1994; **110**:225–240.

Najm H. Uncertainty quantification and polynomial chaos techniques in computational fluid dynamics. *Annu. Rev. Fluid Mech.* 2009; **41**:35–52.

Nakazato R, Park HB, Berman DS, Gransar H, Koo BK, Erglis A, Lin FY, Dunning AM, Budoff MJ, Malpeso J *et al.* Fractional flow reserved derived from computed tomographic angiography (FFRCT) for intermediate severity coronary lesions: results from the DeFACTO trial (determination of fractional flow reserve by anatomic computed tomographic angiography). *J. Am. Coll. Cardiol.* 2012; **60**(17):B6.

Nørgaard BL, Leipsic J, Gaur S, Seneviratne S, Ko BS, Ito H, Jensen JM, Mauri L, De Bruyne B, Bezerra H *et al.* Diagnostic performance of non-invasive fractional flow reserve derived from coronary CT angiography in suspected coronary artery disease: the NXT trial. *J. Am. Coll. Cardiol.* 2014; **63**(12):1145–1155, doi: 10.1016/j.jacc.2013.11.043.

Olufsen M. Structured tree outflow condition for blood flow in larger systemic arteries. *Am. J. Physiol.* 1999; **276**(1):257–268.

Ottesen JT. Modelling of the baroreflex-feedback mechanism with time-delay. *J. Math. Biol.* 1997; **36**(1):41–63.

Ottesen J, Olufsen M and Larsen J. *Applied Mathematical Models in Human Physiology*, Monographs on Mathematical Modeling and Computation. Society for Industrial and Applied Mathematics, 2004.

Peiró J and Veneziani A. Reduced models of the cardiovascular system. In *Cardiovascular Mathematics. Modeling and Simulation of the Circulatory System*, Formaggia L, Quarteroni A and Veneziani A (eds). Springer-Verlag: Milano, 2009; 347–394.

Perktold K, Florian H and Hilbert D. Analysis of pulsatile blood flow: a carotid siphon model. *J. Biomed. Eng.* 1987; **9**(1):46–53.

Perktold K and Hilbert D. Numerical simulation of pulsatile flow in a carotid bifurcation model. *J. Biomed. Eng.* 1986; **8**(3):193–199.

Perktold K, Nerem R and Peter R. A numerical calculation of flow in a curved tube model of the left main coronary artery. *J. Biomech.* 1991a; **24**(3-4):175–189, doi: 10.1016/0021-9290(91)90176-N.

Perktold K, Resch M and Peter RO. Three-dimensional numerical analysis of pulsatile flow and wall shear stress in the carotid artery bifurcation. *J. Biomech.* 1991b; **24**(6):409–420, doi: 10.1016/0021-9290(91)90029-M.

Perktold K and Peter R. Numerical 3D-simulation of pulsatile wall shear stress in an arterial T-bifurcation model. *J. Biomed. Eng.* 1990; **12**(1):2–12.

Perktold K and Rappitsch G. Computer simulation of local blood flow and vessel mechanics in a compliant carotid artery bifurcation model. *J. Biomech.* 1995; **28**:845–856.

Peskin CS. Flow patterns around heart valves: a numerical method. *J. Comput. Phys.* 1972; **10**(2):252–271.

Peskin CS. The immersed boundary method. *Acta Numer.* 2003; **11**:479–517, doi: 10.1017/S0962492902000077.

Petrossian E, Reddy VM, Collins KK, Culbertson CB, MacDonald MJ, Lamberti JJ, Reinhartz O, Mainwaring RD, Francis PD, Malhotra SP *et al.* The extracardiac conduit Fontan operation using minimal approach extracorporeal circulation: early and midterm outcomes. *J. Thorac. Cardiovasc. Surg.* 2006; **132**(5):1054–1063.

Pries A, Reglin B and Secomb T. Structural adaptation of microvascular networks: functional roles of adaptive responses. *Am. J. Physiol. Heart Circ. Physiol.* 2001; **281**(3):H1015–H1025.

Prosi M, Perktold K, Ding Z and Friedman MH. Influence of curvature dynamics on pulsatile coronary artery flow in a realistic bifurcation model. *J. Biomech.* 2004; **37**(11):1767–1775, doi: 10.1016/j.jbiomech.2004.01.021.

Quarteroni A and Rozza G. Optimal control and shape optimization of aorto-coronaric bypass anastomoses. *Math. Models Methods Appl. Sci.* 2003; **13**(12):1801–1823.

Rachev A. A model of arterial adaptation to alterations in blood flow. *J. Elast.* 2000; **61**(1-3):83–111.

Raghu R, Vignon-Clementel IE, Figueroa CA and Taylor CA. Comparative study of viscoelastic arterial wall models in nonlinear one-dimensional finite element simulations of blood flow. *J. Biomech. Eng.* 2011; **133**:1–11, doi: 10.1115/1.4004532.

Ramachandra AB, Kahn AM and Marsden A. Patient specific simulations reveal significant differences in mechanical stimuli in venous and arterial coronary grafts. *J. Cardiovasc. Transl. Res.* 2016; **9**(4):279–290.

Reymond P, Merenda F, Perren F, Rüfenacht D and Stergiopulos N. Validation of a 1-dimensional model of the systemic arterial tree. *Am. J. Physiol. Heart Circ. Physiol.* 2009; **297**(1):H208–H222, doi: 10.1152/ajpheart.00037.2009.

Ross R. Atherosclerosis – an inflammatory disease. *N. Engl. J. Med.* 1999; **340**:115–126.

Ryu K, Healy TM, Ensley AE, Sharma S, Lucas C and Yoganathan AP. Importance of accurate geometry in the study of the total cavopulmonary connection: computational simulations and in vitro experiments. *Ann. Biomed. Eng.* 2001; **29**:844–853.

Sankaran S, Audet C and Marsden A. A method for stochastic constrained optimization using derivative-free surrogate pattern search and collocation. *J. Comput. Phys.* 2010; **229**(12):4664–4682.

Sankaran S, Esmaily-Moghadam M, Kahn A, Tseng E, Guccione J and Marsden A. Patient-specific multiscale modeling of blood flow for coronary artery bypass graft surgery. *Ann. Biomed. Eng.* 2012; **40**(10):2228–2242.

Sankaran S, Humphrey J and Marsden A. An efficient framework for optimization and parameter sensitivity analysis in arterial growth and remodeling computations. *Comput. Methods Appl. Mech. Eng.* 2013; **256**:200–210.

Sankaran S and Marsden A. The impact of uncertainty on shape optimization of idealized bypass graft models in unsteady flow. *Phys. Fluids* 2010; **22**(12):121 902.

Sankaran S and Marsden A. A stochastic collocation method for uncertainty quantification and propagation in cardiovascular simulations. *J. Biomech. Eng.* 2011; **133**(3):031 001.

Schiavazzi DE, Arbia G, Baker C, Hlavacek AM, Hsia TY, Marsden AL and Vignon-Clementel IE. Uncertainty quantification in virtual surgery hemodynamics predictions for single ventricle palliation. *International Journal of Numerical Methods in Biomedical Engineering* 2015; **32**(3):e02737.

Schiavazzi D, Doostan A and Iaccarino G. Sparse multiresolution regression for uncertainty propagation. *Int. J. Uncertainty Quantif.* 2014; **4**(4):303–331.

Scotti CM, Shkolnik AD, Muluk SC and Finol Ea. Fluid-structure interaction in abdominal aortic aneurysms: effects of asymmetry and wall thickness. *Biomed. Eng. Online* 2005; **4**(1):64.

Seeley B and Young D. Effect of geometry on pressure losses across models of arterial stenoses. *J. Biomech.* 1976; **9**(7):439–448, doi: 10.1016/0021-9290(76)90086-5.

Sengupta D, Kahn A, Burns J, Sankaran S, Shadden S and Marsden A. Image-based modeling of hemodynamics and coronary artery aneurysms caused by Kawasaki disease. *Biomech. Model. Mechanobiol.* 2012; **11**(6):915–932.

Serafini DB. A framework for managing models in nonlinear optimization of computationally expensive functions. PhD thesis, Rice University, Houston, TX, 1998.

Sforza DM, Putman CM and Cebral JR. Hemodynamics of cerebral aneurysms. *Annu. Rev. Fluid Mech.* 2009; **41**:91–107.

Sgouralis I and Layton AT. Theoretical assessment of renal autoregulatory mechanisms. *Am. J. Physiol. Renal Physiol.* 2014; **306**(11):F1357–F1371.

Shadden SC and Taylor CA. Characterization of coherent structures in the cardiovascular system. *Ann. Biomed. Eng.* 2008; **36**(7):1152–1162.

Sherwin SJ, Franke V, Peiro J and Parker KH. One-dimensional modelling of a vascular network in space-time variables. *J. Eng. Math.* 2003; **47**(3):217–250, doi: 10.1023/B:ENGI.0000007979.32871.e2.

Simpson TW, Korte JJ, Mauery TM and Mistree F. Comparison of response surface and kriging models for multidisciplinary design optimization. AIAA Paper 98-4755, 1998.

Smith NP. A computational study of the interaction between coronary blood flow and myocardial mechanics. *Physiol. Meas.* 2004; **25**:863–877.

Smith NP, Pullan AJ and Hunter PJ. An anatomically based model of transient coronary blood flow in the heart. *SIAM J. Appl. Math.* 2002; **62**(3):990–1018, doi: 10.1137/S0036139999355199.

Soerensen DD, Pekkan K, de Zelicourt D, Sharma S, Kanter K, Fogel M and Yoganathan A. Introduction of a new optimized total cavopulmonary connection. *Ann. Thorac. Surg.* 2007; **83**(6):2182–2190.

Spilker RL, Feinstein JA, Parker DW, Reddy VM and Taylor CA. Morphometry-based impedance boundary conditions for patient-specific modeling of blood flow in pulmonary arteries. *Ann. Biomed. Eng.* 2007; **35**(4):546–549.

Steinman DA, Hoi Y, Fahy P, Morris L, Walsh MT, Aristokleous N, Anayiotos AS, Papaharilaou Y, Arzani A, Shadden SC *et al.* Variability of computational fluid dynamics solutions for pressure and flow in a giant aneurysm: the ASME 2012 summer bioengineering conference CFD challenge. *J. Biomech. Eng.* 2013; **135**(2):21 016.

Stergiopulos N, Young DF and Rogge TR. Computer simulation of arterial flow with applications to arterial and aortic stenoses. *J. Biomech.* 1992; **25**(12):1477–1488.

Stewart SFC, Paterson EG, Burgreen GW, Hariharan P, Giarra M, Reddy V, Day SW, Manning KB, Deutsch S, Berman MR *et al.* Assessment of CFD performance in simulations of an idealized medical device: results of FDA's first computational interlaboratory study. *Cardiovasc. Eng. Technol.* 2012; **3**(2):139–160.

Taber LA. A model for aortic growth based on fluid shear and fiber stresses. *J. Biomech. Eng.* 1998; **120**(3):348–354.

Tang BT, Cheng CP, Draney MT, Wilson NM, Tsao PS, Herfkens RJ and Taylor CA. Abdominal aortic hemodynamics in young healthy adults at rest and during lower limb exercise: quantification using image-based computer modeling. *Am. J. Physiol. Heart Circ. Physiol.* 2006; **291**:H668–H676.

Tang BT, Fonte TA, Chan FP, Tsao PS, Feinstein JA and Taylor CA. Three-dimensional hemodynamics in the human pulmonary arteries under resting and exercise conditions. *Ann. Biomed. Eng.* 2011; **39**(1):347–358.

Taylor CA, Cheng CP, Espinosa LA, Tang BT, Parker D and Herfkens RJ. In vivo quantification of blood flow and wall shear stress in the human abdominal aorta during lower limb exercise. *Ann. Biomed. Eng.* 2002; **30**(3):402–408.

Taylor CA, Fonte T and Min J. Computational fluid dynamics applied to cardiac CT for noninvasive quantification of fractional flow reserve: scientific basis. *J. Am. Coll. Cardiol.* 2013; **61**(22):2233–2241.

Taylor CA, Hughes TJR and Zarins CK. Computational investigations in vascular disease. *Comput. Phys.* 1996; **10**(3):224–232.

Taylor CA, Hughes TJR and Zarins CK. Finite element modeling of 3-dimensional pulsatile flow in the abdominal aorta: relevance to atherosclerosis. *Ann. Biomed. Eng.* 1998a; **26**(6):1–13.

Taylor CA, Hughes TJR and Zarins CK. Finite element modeling of blood flow in arteries. *Comput. Methods Appl. Mech. Eng.* 1998b; **158**:155–196.

Taylor CA, Hughes TJR and Zarins CK. Effect of exercise on hemodynamic conditions in the abdominal aorta. *J. Vasc. Surg.* 1999; **29**(6):1077–1089.

Torczon V. On the convergence of pattern search algorithms. *SIAM J. Optim.* 1997; **7**:1–25.

Torii R, Keegan J, Wood NB, Dowsey AW, Hughes AD, Yang GZ, Firmin DN, Thom SAM and Xu XY. Mr image-based geometric and hemodynamic investigation of the right coronary artery with dynamic vessel motion. *Ann. Biomed. Eng.* 2010; **38**:2606–2620.

Tune J, Richmond K, Gorman M and Feigl E. Control of coronary blood flow during exercise. *Exp. Biol. Med.* 2002; **227**(4):238–250.

Updegrove A, Wilson NM, Merkow J, Lan H, Marsden AL and shadden SC. SimVascular: an open source pipeline for cardiovascular simulation. *Ann. Biomed. Eng.* 2016; **45**(3):525–541.

Ursino M. A mathematical study of human intracranial hydrodynamics Part 1-the cerebrospinal fluid pulse pressure. *Ann. Biomed. Eng.* 1988; **16**(4):379–401.

Ursino M and Lodi CA. A simple mathematical model of the interaction between intracranial pressure and cerebral hemodynamics. *J. Appl. Physiol.* 1997; **82**(4):1256–1269.

Ursino M, Lodi CA, Alberto C and Interaction L. Interaction among autoregulation, CO2 reactivity, and intracranial pressure: a mathematical model. *Am. J. Physiol. Heart Circ. Physiol.* 1998; **274**(51):1715–1728.

Valdez-Jasso D, Bia D, Zócalo Y, Armentano RL, Haider MA and Olufsen MS. Linear and nonlinear viscoelastic modeling of aorta and carotid pressure–area dynamics under in vivo and ex vivo conditions. *Ann. Biomed. Eng.* 2011; **39**(5):1438–1456, doi: 10.1007/s10439-010-0236-7.

Valentín A and Humphrey JD. Evaluation of fundamental hypotheses underlying constrained mixture models of arterial growth and remodelling. *Philos. Trans. R. Soc. London, Ser. A* 2009; **367**(1902):3585–3606.

van de Vosse FN, de Hart J, Van Oijen CHGA, Bessems D, Gunther TWM, Segal A, Wolters BJBM, Stijnen JMA and Baaijens FPT. Finite-element-based computational methods for cardiovascular fluid-structure interaction. *J. Eng. Math.* 2003; **47**(3-4):335–368.

van Loon R, Anderson PD and van de Vosse FN. A fluid-structure interaction method with solid-rigid contact for heart valve dynamics. *J. Comput. Phys.* 2006; **217**(2):806–823.

Vankan J, Huyghe JM, Janssen D, Huson A, Hacking WJG and Schreiner W. Finite element analysis of blood flow through biological tissue. *Int. J. Eng. Sci.* 1997; **35**:375–385.

Vigmond EJ, Clements C, McQueen DM and Peskin CS. Effect of bundle branch block on cardiac output: a whole heart simulation study. *Prog. Biophys. Mol. Biol.* 2008; **97**(2-3):520–542.

Vignon-Clementel IE, Figueroa CA, Jansen KE and Taylor CA. Outflow boundary conditions for three-dimensional finite element modeling of blood flow and pressure in arteries. *Comput. Methods Appl. Mech. Eng.* 2006; **195**:3776–3796. doi: 10.1016/j.cma.2005.04.014

Vignon-Clementel IE, Figueroa CA, Jansen KE and Taylor CA. Outflow boundary conditions for three-dimensional simulations of non-periodic blood flow and pressure fields in deformable arteries. *Comput. Methods Biomech. Biomed. Eng.* 2010; **13**(5):625–640.

Vukicevic M, Chiulli JA, Conover T, Pennati G, Hsia TY and Figliola RS. Mock circulatory system of the fontan circulation to study respiration effects on venous flow behavior. *Comput. Methods Appl. Mech. Eng.* 2013; **59**(3):253–260.

Watton P, Hill N and Heil M. A mathematical model for the growth of the abdominal aortic aneurysm. *Biomech. Model. Mechanobiol.* 2004; **3**:98–113, doi: 10.1007/s10237-004-0052-9.

Watton PN, Luo XY, Wang X, Bernacca GM, Molloy P and Wheatley DJ. Dynamic modelling of prosthetic chorded mitral valves using the immersed boundary method. *J. Biomech.* 2007; **40**(3):613–626.

Westerhof N, Bosman F, De Vries CJ and Noordergraaf A. Analog studies of the human systemic arterial tree. *J. Biomech.* 1969; **2**:121–143.

Westerhof N, Lankhaar J and Westerhof BE. The arterial windkessel. *Med. Biol. Eng. Comput.* 2009; **47**(2):131–141.

Whitehead KK, Pekkan K, Kitahima HD, Paridon SM, Yoganathan AP and Fogel MA. Nonlinear power loss during exercise in single-ventricle patients after the Fontan: insights from computational fluid dynamics. *Circulation* 2007; **116**:I–165–I–171.

Wilson N, Wang K, Dutton R and Taylor CA. A software framework for creating patient specific geometric models from medical imaging data for simulation based medical planning of vascular surgery. *Lect. Notes Comput. Sci.* 2001; **2208**:449–456.

Wolters BJBM, Rutten MCM, Schurink GWH, Kose U, de Hart J and van de Vosse FN. A patient-specific computational model of fluid-structure interaction in abdominal aortic aneurysms. *Med. Eng. Phys.* 2005; **27**(10):871–883, doi: 10.1016/j.medengphy.2005.06.008.

Xi J, Lamata P, Lee J, Moireau P, Chapelle D and Smith N. Myocardial transversely isotropic material parameter estimation from in-silico measurements based on a reduced-order unscented Kalman filter. *J. Mech. Behav. Biomed. Mater.* 2011; **4**(7):1090–1102.

Xiao N, Alastruey J and Figueroa CA. A systematic comparison between 1-D and 3-D hemodynamics in compliant arterial models. *Int. J. Numer. Methods Biomed. Eng.* 2014; **30**(2): 204–231. doi: 10.1002/cnm.2598

Xiao N, Humphrey JD and Figueroa CA. Multi-scale computational model of three-dimensional hemodynamics within a deformable full-body arterial network. *J. Comput. Phys.* 2013; **244**:22–40, doi: 10.1016/j.jcp.2012.09.016.

Xiu D and Hesthaven J. High-order collocation methods for differential equations with random inputs. *SIAM J. Sci. Comput.* 2005; **27**(3):1118–1139.

Yang W, Feinstein J and Marsden A. Constrained optimization of an idealized Y-shaped baffle for the fontan surgery at rest and exercise. *Comput. Methods Appl. Mech. Eng.* 2010; **199**(33):2135–2149.

Yang W, Feinstein JA, Shadden S, Vignon-Clementel I and Marsden AL. Optimizatin of a Y-graft design for improved hepatic flow distribution in the fontan circulation. *J. Biomech. Eng.* 2013; **135**(1):011002.

Yang W, Vignon-Clementel I, Troianowski G, Reddy V, Feinstein JA and Marsden AL. Hepatic blood flow distribution and performance in traditional and Y-graft Fontan geometries: a case series computational fluid dynamics study. *J Thorac Cardiovasc Surg.* 2012; **143**(5):1086–1097. doi: 10.1016/j.jtcvs.2011.06.042. Epub 2011 Sep 29.

Young DF and Tsai FY. Flow characteristics in models of arterial stenoses – II. Unsteady flow. *J. Biomech.* 1973; **6**(5):547–559.

Zarins C, Giddens D, Bharadvaj B, Sottiurai V, Mabon R and Glagov S. Carotid bifurcation atherosclerosis. Quantitative correlation of plaque localization with flow velocity profiles and wall shear stress. *Circ. Res.* 1983; **53**(4):502–514.

Zarins C, Zatina M, Giddens DP, Ku DN and Glagov S. Shear stress regulation of artery lumen diameter in experimental atherogenesis. *J. Vasc. Surg.* 1987; **5**:413–420.

Zhang Y, Bazilevs Y, Goswami S, Bajaj C and Hughes T. Patient-specific vascular NURBS modeling for isogeometric analysis of blood flow. *Comput. Methods Appl. Mech. Eng.* 2007; **196**(29-30):2943–2959.